Published in final edited form as:

Cell Rep. 2022 May 31; 39(9): 110874. doi:10.1016/j.celrep.2022.110874.

Cholinergic interneurons mediate cocaine extinction in male mice through plasticity across medium spiny neuron subtypes

Weston Fleming[1], **Junuk Lee**[1,3], **Brandy A. Briones**[1,2], **Scott S. Bolkan**[1], **Ilana B. Witten**[1,2,3,4,*]

[1]Princeton Neuroscience Institute, Princeton, NJ 08544, USA

[2]Department of Psychology, Princeton University, Princeton, NJ 08544, USA

[3]Senior author

[4]Lead contact

SUMMARY

Cholinergic interneurons (ChINs) in the nucleus accumbens (NAc) have been implicated in the extinction of drug associations, as well as related plasticity in medium spiny neurons (MSNs). However, since most previous work relied on artificial manipulations, whether endogenous acetylcholine signaling relates to drug associations is unclear. Moreover, despite great interest in the opposing effects of dopamine on MSN subtypes, whether ChIN-mediated effects vary by MSN subtype is also unclear. Here, we find that high endogenous acetylcholine event frequency correlates with greater extinction of cocaine-context associations across male mice. Additionally, extinction is associated with a weakening of glutamatergic synapses across MSN subtypes. Manipulating ChIN activity bidirectionally controls both the rate of extinction and the associated plasticity at MSNs. Our findings indicate that NAc ChINs mediate drug-context extinction by reducing glutamatergic synaptic strength across MSN subtypes, and that natural variation in acetylcholine signaling may contribute to individual differences in extinction.

Graphical abstract

*Correspondence: iwitten@princeton.edu.

AUTHOR CONTRIBUTIONS

Conceptualization, W.F., J.L., I.B.W.; Methodology, W.F., J.L., B.B., S.B., I.B.W.; Validation, W.F., J.L., B.B., S.B.; Investigation, W.F.; Formal analysis, W.F., J.L.; Writing - Original draft, W.F., I.B.W.; Writing - Review and editing, W.F., J.L., B.B., S.B., I.B.W.; Visualization, W.F.; Resources, I.B.W.; Supervision, J.L., I.B.W.; Funding acquisition, W.F., I.B.W.

SUPPLEMENTAL INFORMATION

Supplemental information can be found online at https://doi.org/10.1016/j.celrep.2022.110874.

DECLARATION OF INTERESTS

The authors declare no competing interests.

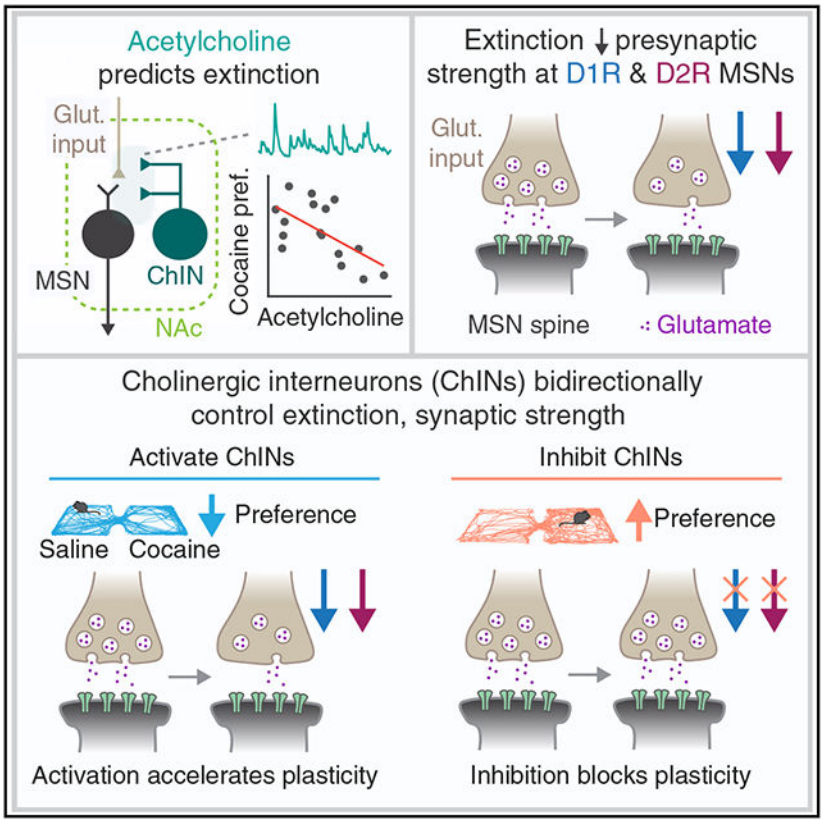

In brief

Fleming et al. show that individual differences in nucleus accumbens (NAc) acetylcholine signaling correlate with extinction of a cocaine-context association. Manipulations of NAc cholinergic interneuron activity support a model where acetylcholine release weakens glutamatergic presynaptic strength at NAc D1R and D2R medium spiny neurons, promoting cocaine-context extinction.

INTRODUCTION

Animals must update reward-context associations when a reward is no longer present, a process known as extinction. Understanding the neural mechanisms of extinction is not only of fundamental relevance, but also of potential clinical relevance. Drugs like cocaine can form persistent drug-context associations, and understanding the mechanisms that underlie their extinction may offer insight to treatments that promote abstinence.

Key neural processes that contribute to the formation and extinction of drug-context associations are believed to occur in the NAc. Addictive drugs generate high levels of dopamine (DA) release in the NAc. As a result, the role of DA in addiction-related NAc plasticity has been studied extensively (Britt et al., 2012; Kourrich et al., 2007; MacAskill et al., 2014; Pascoli et al., 2014; Robinson et al., 2001).

In addition, there is growing appreciation for a complementary role of acetylcholine (ACh) — a comparatively understudied neuromodulator in the NAc—in regulating plasticity and drug-context learning (Aitta-Aho et al., 2017; Collins et al., 2019; Lee et al., 2016; Witten et al., 2010). However, since previous work has relied primarily on artificial manipulation of cholinergic interneurons (ChINs), whether natural variation in ACh across individuals is predictive of drug associations and their persistence is unknown.

Another open question is whether and how ChINs differentially modulate the output populations of the NAc to drive extinction of drug-context associations. The NAc is composed principally of medium spiny neurons (MSNs), which function as the structure's primary output and can be classified into two subtypes by the DA receptor expressed (either D1R or D2R). DA supports different forms of plasticity in these two MSN subtypes (Gerfen et al., 1990; Iino et al., 2020; Lee et al., 2021; Shen et al., 2008), a phenomenon believed to contribute to the distinct and sometimes opposing roles these sub-populations have in reward-related behaviors (Bock et al., 2013; Cole et al., 2018; Durieux et al., 2009; Gallo et al., 2018; Hikida et al., 2010; Kravitz et al., 2012; Lobo et al., 2010; O'Neal et al., 2020). It is possible that ChIN activity also produces MSN subtype-specific plasticity, given the different muscarinic receptor expression profiles across MSN cell types (Bernard et al., 1992; Lim et al., 2014; Yan et al., 2001), and given ACh's ability to mediate DA release onto MSNs (Cachope et al., 2012; Threlfell et al., 2012; Yorgason et al., 2017). Alternatively, ChINs may drive similar changes across MSN subtypes, given that MSNs are driven by input from glutamatergic projections (Britt et al., 2012; Phillipson and Griffiths, 1985) that express muscarinic receptors (Hernández-Echeagaray et al., 1998; Higley et al., 2009; Sugita et al., 1991) and that are inhibited similarly by muscarinic activation *ex vivo* (Ding et al., 2010).

To address these gaps, we extend a previous observation (Lee et al., 2016) that artificial activation of ChINs enhances cocaine-context extinction by demonstrating a role for natural variations in ACh in mediating individual differences. Specifically, we use an ACh indicator to demonstrate that the frequency of ACh events is predictive of the strength and persistence of cocaine-context associations across individuals. We also show that cocaine extinction is associated with a decrease in glutamatergic presynaptic strength on NAc MSNs, and the activation or inhibition of ChIN activity bidirectionally controls this synaptic strength at both MSN subtypes. Taken together, this implies that elevated ChIN activity hastens extinction by accelerating naturally occurring plasticity mechanisms across MSN subtypes.

RESULTS

Repeat extinction after cocaine conditioned place preference decreases excitatory transmission at both D1R and D2R MSNs

Before characterizing the correlates and consequences of NAc ACh during cocaine-context extinction, we first sought to identify the extinction-dependent changes in glutamatergic synaptic strength at D1R and D2R MSNs.

To study plasticity changes related to drug-context extinction, we conditioned and extinguished male mice through a cocaine conditioned place preference (CPP). During the

first day of the CPP (baseline), mice had access to both zones of the CPP chamber. The next 2 days, mice underwent conditioning, during which one zone was paired with cocaine (15 mg/kg, i.p.) and the other with saline. One group of mice (repeat extinction) underwent 4 subsequent days of post-conditioning tests (tests 1–4) to assess and extinguish their preference (Quirk and Mueller, 2008; Rescorla, 2001). Since plasticity has been observed after cocaine experience (Boudreau, 2005; Boudreau et al., 2007; Ferrario et al., 2011; Ghasemzadeh et al., 2009; Kourrich et al., 2007; Thomas et al., 2001, 2008), to control for time-dependent changes, a separate group (no extinction) was conditioned but did not undergo extinction testing (Figure 1A). As expected, mice that underwent repeat extinction testing showed a preference for the cocaine zone on test 1, which decreased on tests 2–4 (Figure 1B). In a separate group of behavior-only control mice, we confirmed that CPP was preserved to the day 7 time point if mice did not undergo extinction testing prior (Figure 1B; test 4 control).

To assess how extinction affected glutamatergic synaptic strength at MSNs in NAc medial shell, brain slices were taken on day 7 and mini excitatory postsynaptic currents (mEPSCs) were recorded (Figures 1C and 1D). We used drd1a-tdTomato and drd2-GFP mice used to target recordings to each MSN subtype after first validating that the lines display high degrees of specificity and penetrance (Figure S1).

Mice that underwent extinction showed decreased mEPSC frequencies at both D1R and D2R MSNs compared with controls (Figures 1E and 1F), suggesting that extinction weakens presynaptic glutamatergic strength. In contrast, there was no significant effect on amplitudes at either MSN population (Figures 1G and 1H). This decrease in synaptic strength with extinction was not a reversal of a synaptic strengthening process during conditioning (Figure S1), consistent both with previous studies that have not observed potentiation in glutamatergic synaptic strength within 24 h of a final cocaine exposure (Kourrich et al., 2007) and with learning models positing that extinction is a new learning process rather than erasure of the previous association (Bouton, 2004; Pavlov, 1960; Robbins, 1990).

To confirm the presynaptic origins of the plasticity effects associated with extinction, we performed additional experiments in which glutamatergic afferents onto NAc MSNs were electrically stimulated and evoked EPSCs were measured. We performed paired pulse ratio (PPR) measurements as an assay of presynaptic strength (Choi and Lovinger, 1997; Tang et al., 2001) (Figures 1C and 1I). Mice that underwent extinction showed significant enhancement of PPRs at both D1R and D2R MSNs compared with controls (Figures 1J and 1K), consistent with the observed decrease in mEPSC frequencies (Figures 1E and 1F). Together, these findings show that extinction involves a decrease in presynaptic strength in excitatory transmission onto both D1R and D2R MSNs in NAc.

Higher ACh event rate during cocaine extinction is associated with lower cocaine preference and persistence

We next examined how endogenous ACh release relates to cocaine CPP acquisition and extinction. Toward this end, we injected a $GRAB_{ACh}$ sensor (AAV2/9-hSyn-GACh3.0) (Jing et al., 2020) into the medial shell of NAc to record ACh levels during cocaine CPP (Figures 2A and 2B; fiber locations in Figure S2), after first confirming *ex vivo* that the indicator was

selectively activated by ACh (Figure 2C). Mice underwent cocaine CPP followed by 4 days of extinction (Figure 2D). During cocaine conditioning, there was a significant decrease in ACh event frequency and amplitude compared with saline conditioning (Figure 2E; Figure S3). After conditioning, mice showed a significant preference for the cocaine zone that decreased with subsequent tests, indicating extinction learning (Figure S4).

On the first extinction test after conditioning (test 1), there was a significant decrease in ACh event frequency compared with baseline (Figures 2F and 2G; Figure S4). This decrease was only evident in the behavioral chamber and not during the periods immediately before or after, when the mouse was in its home cage (Figures 2F and 2G). Event frequency was similar regardless of chamber side (Figure 2H), was not dependent on recording fiber placement (Figure S2), and showed similar modulation during entries to either zone (Figure S4).

Given the decrease in ACh event frequency during test 1, and given that manipulation of ChIN activity modulates cocaine CPP extinction (Lee et al., 2016), we wondered if individual differences in ACh during test 1 may be related to the trajectory of extinction learning. Specifically, we hypothesized that higher ACh event frequencies at test 1 would promote acquisition of the extinction memory, and thus be predictive of weaker, less persistent cocaine-context associations. Indeed, we found that ACh event frequency on test 1 was negatively correlated with cocaine preference across days (Figures 2I–2K and S4). Thus, heightened ACh at test 1 is associated with weaker, less persistent cocaine preference. In contrast, ACh event frequency during cocaine conditioning was not predictive of ACh event frequency during test 1 and had limited predictive power of preference (Figure S3).

We also examined the relationship between ACh events and locomotion. Activity in ChINs is not thought to have a consistent relationship with locomotion in NAc (Howe et al., 2019). However, because ChIN activity is associated with reward-related events (Aosaki et al., 1994; Apicella, 2017; Apicella et al., 1991; Dorst et al., 2020; Joshua et al., 2008; Morris et al., 2004), and because cocaine increases locomotion, we wondered whether conditioning would enhance the relationship between NAc ACh and locomotion. Indeed, we observed a post-conditioning change in the relationship between an animal’s speed and the timing of ACh events. Specifically, while speed was similar before versus after conditioning (Figure 3A), and ACh events had little relation to speed before conditioning (Figure 3B), there was a decrease in speed at the time of ACh events after versus before conditioning (Figures 3C and 3D). This relationship was similar in the cocaine and saline zone (Figure 3C), but was not evident in mice that received saline-only conditioning (Figure S5). Consistent with this relationship between speed and ACh events, after conditioning, higher speeds were more negatively associated with ACh event frequencies (Figure 3E).

Finally, we asked whether individual variability in this ACh-speed relationship may predict CPP extinction. Indeed, mice with a stronger relationship between speed and ACh event rates after conditioning exhibited less persistent cocaine preference (i.e., stronger extinction) (Figures 3E, 3F, and S5). In contrast with this association with extinction, preference on test 1 was not predicted by the relationship between speed and ACh events. This effect was not driven by a relationship between extinction and speed (Figure S5). This cocaine-conditioned

motor correlate, and its striking relationship to extinction, strengthen the general connection between ACh and cocaine extinction, although the underlying mechanisms are unclear.

Taken together, stronger cocaine preference across individuals is predicted by low ACh event rates after conditioning (Figures 2J and 2K) and a tendency for the remaining events to occur at times of higher speed (Figures 3E and 3F).

Inhibition of ChINs blocks extinction and the associated reduction of excitatory synaptic strength at MSNs

We next sought to determine if there was a connection between the observed relationship between NAc ACh event rates and extinction (Figures 2J and 2K) and the decrease in excitatory synaptic strength at NAc MSNs owing to extinction (Figures 1E–1K).

To this end, during extinction, we inhibited ChINs using the designer receptor exclusively activated by designer drug hM4D(G_i) (G_i-DREADD) (Armbruster et al., 2007). To confirm that G_i-DREADD inhibition decrease ACh events *in vivo* (Aitta-Aho et al., 2017; Laverne et al., 2021; Lewis et al., 2020), we co-injected a ChAT::Cre mouse with an adeno-associated virus (AAV)5 virus-expressing Cre-dependent hM4D(G_i)-mCherry and GACh3.0 (Figure 4A), and found that the frequency and amplitude of ACh events were decreased 30 min after clozapine *N*-oxide (CNO) injection (Figures 4B and 4C).

To virally target ChINs for manipulation during behavior and identify MSNs by subtype during subsequent *ex vivo* electrophysiology experiments, we used ChAT::Cre mice crossed with either drd1a-tdTomato or drd2-GFP mice (Figure S1). Cre-dependent hM4D(G_i)-mCherry was injected bilaterally into the medial shell of NAc in one group, while control mice received Cre-dependent mCherry virus (Figure 4D). Mice underwent cocaine CPP and repeat extinction (Figure 4E), and both groups received injections of CNO (3.0 mg/kg, i.p.) 30 min before each extinction test.

We predicted that G_i-DREADD mice would show preserved preference for the cocaine zone and increased excitatory synaptic strength compared with controls after repeat extinction. Although preference during test 1 was similar between groups, over tests 2–4, G_i-DREADD mice indeed showed more preference for the cocaine side than did controls, consistent with decreased extinction learning (Figure 4F). G_i-DREADD activation did not alter locomotion compared with controls (Figure 4G).

Immediately after extinction testing, brain slices were collected to measure mEPSCs to determine whether inhibiting ChINs during extinction testing blocked the reduction of synaptic strength we observed after repeat extinction (Figures 1E and 1F). G_i-DREADD mice did indeed have significantly higher mEPSC frequencies at D1R MSNs and D2R MSNs than did controls (Figures 4H–4J). There was no difference in mEPSC amplitude between groups in either cell type (Figures 4K and 4L). These data support the importance of endogenous ChIN activity in the decrease of glutamatergic synaptic strength across NAc MSNs that accompanies repeat extinction.

Activation of ChINs during a single extinction test generates decreases in excitatory synaptic strength across MSN subtypes, mimicking changes that occur during repeat extinction

To complement our finding that the inhibition of ChINs prevented extinction and the associated presynaptic plasticity onto MSNs (Figure 4), we next sought to determine if activation of ChINs during a single extinction session would hasten extinction and the associated plasticity.

To activate ChINs during extinction testing, an AAV2/5 virus expressing Cre-dependent ChR2-YFP was injected into the medial shell of NAc of double transgenic mice (ChAT::Cre×drd1a-tdTomato or ChAT::Cre×drd2-GFP), and optical fibers were implanted bilaterally above the structure (Figures 5A and 5B; Figure S6). Mice underwent cocaine CPP, and on day 4 (test) underwent an extinction test (Figure 5C). For the duration of this test, mice received phasic optogenetic stimulation of ChINs (ChIN activation; 15 Hz, 2 s on, 2 s off) (Lee et al., 2016) (Figure 5B). Stimulation was not dependent on chamber side, as we did not observe differences in ACh event rate based on chamber side (Figure 2H).

Consistent with our indicator data (Figures 2J and 2K) and the ChIN inhibition experiment (Figure 4F), as well as previous optogenetic manipulations (Lee et al., 2016), mice that received activation of ChINs during testing showed significantly less preference for the cocaine zone compared with controls (Figures 5D and 5E; Figure S7). The difference in preference between groups emerged during the course of the test session (Figure 5F), suggesting that ChIN activation accelerates extinction.

Immediately after extinction testing, brain slices were collected for plasticity measurements (Figure 5C). We first measured mEPSCs to determine whether activation of ChINs generated decreases in mEPSC frequency as seen after repeat extinction (Figure 5G). Indeed, compared with controls, mice who received ChIN activation during extinction testing had significantly lower mEPSC frequencies at both D1R and D2R MSNs (Figures 5H and 5I; Figure S7). The mEPSC frequencies after ChIN activation were similar to those seen following repeat extinction (Figures S7). In addition, ChIN activation decreased mEPSC amplitudes at D2R MSNs (Figures 5J and 5K). This suggests ChIN activation during extinction causes presynaptic weakening on both cell types and postsynaptic weakening on D2R MSNs.

To confirm the pre- and postsynaptic sites of these plasticity effects, we performed additional experiments in which evoked EPSCs in NAc MSNs were measured in response to stimulation of glutamatergic afferents. We first measured PPRs (Figure 5L). Mice that received ChIN activation during extinction testing showed significant enhancement of PPRs at D1R and D2R MSNs compared with controls (Figures 5M and 5N), consistent with the observed decrease in mEPSC frequencies (Figures 5H and 5I). Next, alpha-amino-3-hydroxy-5-methyl-4-isoxazole propionic acid (AMPA) and *N*-methyl-D-aspartate (NMDA) receptor currents were measured (Figure 5O). At D2R MSNs, ChIN activation produced a significant reduction in AMPA/NMDA ratio compared with controls (Figures 5P and 5Q), consistent with the observed reduction in D2R MSN mEPSC amplitudes (Figures 5J and 5K). Taken together, these experiments show that ChIN activation promotes extinction of

cocaine CPP through a combination of pre- and post-synaptic plasticity effects that dampen glutamatergic transmission at both D1R and D2R MSNs.

As another readout of postsynaptic plasticity, we also examined whether *in vivo* ChIN activation affected the temporal summation of glutamatergic inputs. This experiment was motivated by a previous study that found that *ex vivo* muscarine treatment enhanced temporal summation in D2R MSNs (Shen et al., 2007). To test for such effects of ChIN activity *in vivo* during extinction, we repeatedly and rapidly iontophoretically delivered glutamate onto visually identified dendrites of D2R MSNs (Figure 5R). In contrast with the previous study, ChIN activation during extinction testing decreased temporal summation of EPSPs (Figure 5S). This further supports our observation that ChIN activation during extinction decreases the excitatory influence of glutamatergic signals arriving at D2R MSNs.

Activation of ChINs during extinction produces small effects on membrane excitability in MSNs

We also examined whether ChIN activity during extinction may affect MSN membrane excitability (Figure 5T). Cells were recorded in current clamp at resting potentials of approximately −80 mV while current steps were injected. In comparing the number of spikes evoked by the amount of current injected, there was a small but significant interaction between ChIN activation and current at both the D1R and D2R MSNs, indicating a decrease in excitability (Figure 5U). There was no effect of ChIN activation on the action potential threshold, spike amplitude, first inter-spike interval, or after hyperpolarization statistics for either MSN subtype. Moreover, ChIN activation decreased latency to spike in D1R MSNs (Figure S7), a form of increased excitability. Thus, while ChIN activation has profound effects in weakening glutamatergic synaptic strength, it produces comparatively subtle effects on MSN membrane excitability.

DISCUSSION

Here, we first demonstrate that cocaine-context extinction decreases excitatory synaptic strength across MSN subtypes in the NAc. During an initial extinction test, individual differences in *in vivo* ACh event frequency are correlated with the extinction of a cocaine preference. Consistent with these correlates, manipulations of NAc ChIN activity bidirectionally control cocaine-context extinction and associated plasticity. Together, our findings point to a model where ChIN activity promotes drug-context extinction by weakening glutamatergic projections onto both D1R and D2R MSNs. This mechanism may explain how natural variation in NAc ACh contributes to individual differences in drug-context extinction.

Individual variability in ACh predicts the strength and persistence of cocaine-context associations

While there is growing appreciation that ACh plays an important role in drug associations,whether differences in the *in vivo* patterns of ACh across individuals are predictive of the strength and persistence of drug associations was unclear. Previous work suggests that individual differences in phasic DA after drug exposure are predictive of

drug-seeking behavior (Juarez et al., 2017; Willuhn et al., 2014). Our work suggests that ACh may also determine individual differences in drug associations, as we observed that mice with lower ACh event rates have longer lasting cocaine-context associations, consistent with the effects of manipulating ChIN activity. This could imply that individuals with ChIN circuitry that is more dysregulated after drug taking may struggle to extinguish drug-context associations, making them vulnerable to context-induced drug taking. As our experiment used a brief drug conditioning paradigm, a remaining question is whether chronic drug exposure would generate longer-lasting changes in ACh.

We found the clearest relationship between ACh and the progression of extinction during the first extinction test (Figure 2). Conceptually, this is a unique time point, as it involves both the first retrieval and expression of the cocaine-context memory and the initial acquisition (and possibly expression) of the extinction memory. If there is competition between the expression of the cocaine memory and acquisition of the extinction memory, then this first test may be pivotal for determining to what extent a given mouse will extinguish over the following days.

The ACh events we detect *in vivo* may be the product of coordinated spike responses between multiple ChINs. Neighboring ChINs are known to exhibit synchronous activity (Ding et al., 2010; Howe et al., 2019). Synchronized bursts are important for modulating NAc circuit activity and plasticity, causing local release of DA (Cachope et al., 2012; Threlfell et al., 2012) and suppressing MSN activity (English et al., 2011; Witten et al., 2010). That ACh events may represent synchronous firing would explain why we observed decreases in this measure during acute cocaine, while ChIN firing rates are believed to increase during acute cocaine exposure (Berlanga et al., 2003; Lee et al., 2020; Witten et al., 2010).

What might underlie variability in ACh event frequencies across mice? There are multiple mechanisms by which drug exposure may influence ChIN activity. A recent study showed that mice susceptible to cocaine seeking exhibited a higher expression of inhibitory D2Rs on ChINs themselves (Lee et al., 2020). Another study demonstrated that DA can desynchronize ChIN activity via action at D2Rs (Dorst et al., 2020). Taken together, these studies implicate DA's potential to desynchronize ChIN activity as a factor in addiction susceptibility. Additionally, it has been shown that, in the NAc medial shell, a single dose of amphetamine decreases the burst response ChINs exhibit in response to DA terminal stimulation by attenuating glutamate co-release (Chuhma et al., 2014), an example of how excitatory input onto ChINs can undergo rapid modification. Recent work has also demonstrated the importance of GABAergic projections from the ventral tegmental area onto ventral NAc ChINs in promoting reward reinforcement (Al-Hasani et al., 2021), but whether these projections undergo drug-related plasticity is unknown.

Whether the relationship between ACh and extinction generalizes to natural rewards is an open question. Our observation that ACh event frequency was decreased during the first extinction test only when the animal was in the behavior chamber suggests that this decrease may be a conditioned response to the chamber, distinct from the decrease seen during acute cocaine use, which may be driven by pharmacological action more specific to cocaine.

Thus, it is possible that a context-induced decrease in ACh events after reward-context conditioning is a phenomenon that would generalize to other drug and natural rewards.

Finally, while NAc ACh is not believed to have strong motor correlates (Howe et al., 2019), we observed that cocaine CPP produced a distinct relationship between ACh events and speed (Figure 3). Surprisingly, a stronger post-conditioning relationship between ACh event frequency and speed predicted stronger extinction. Why this relationship is predictive of extinction is unclear, but it may allude to the balance of DA and ACh during extinction. DA and ACh may have opposing influences on motor output, promoting and inhibiting activity, respectively (Bordia et al., 2016; Howe and Dombeck, 2016; Kaneko et al., 2000; Kondabolu et al., 2016; Maurice et al., 2015; Ztaou et al., 2016). If DA levels are lower after cocaine conditioning in a given mouse, ACh may be more influential on motor output, leading to a more prominent ACh-speed relationship. The same mouse may have enhanced extinction if lower DA levels are more effectively signaling an absence of reward. This hypothesis—that the ACh-speed relationship indirectly indicates the balance of ACh and DA—would be testable with simultaneous ACh and DA measurement during cocaine CPP.

Weakening of glutamatergic inputs across MSN subtypes in NAc is a key component of extinction

Our results support the idea that weakening glutamatergic inputs onto both MSN subtypes in NAc is a key extinction mechanism, and that endogenous ACh contributes to this change. The observation of similar presynapatic plasticity during cocaine extinction on both MSN subtypes is somewhat surprising in light of the sometimes opposing contributions they have on reward-related behaviors. What might be the functional significance of this observation of similar plasticity on both MSN subtypes as a result of cocaine extinction and of ChIN activation? One possibility relates to how MSN activity changes with cocaine CPP: D1R MSNs show increased activity before entry into the cocaine zone (Calipari et al., 2016), and D2R MSNs preferentially fire in the cocaine zone (Sjulson et al., 2018). In a simple model, it may be that extinction requires the weakening of inputs at D1R MSNs to decrease likelihood of cocaine zone entry and the weakening of inputs at D2R MSNs to decrease the likelihood that the animal remains in the cocaine zone. Mechanistically, the nonspecific decrease in presynaptic glutamatergic strength at MSNs may relate to *in vitro* experiments demonstrating that acute muscarinic activation inhibits glutamatergic afferents across MSN subtypes (Barral et al., 1999; Ding et al., 2010; Malenka and Kocsis, 1988; Pakhotin and Bracci, 2007) via action at M2- and M3-type muscarinic receptors on these afferents (Hernández-Echeagaray et al., 1998; Higley et al., 2009; Sugita et al., 1991).

In addition to the shared presynaptic plasticity across MSN subtypes, we also observed a D2R MSN-specific postsynaptic weakening following ChIN activation that was not seen in the repeat extinction experiments. This difference may be because the optogenetic stimulation generates ACh levels not reached endogenously.

Limitations of the study

Sex differences can also affect drug learning. Female mice show estrous-dependent enhancements in DA neuron bursting that strengthen cocaine CPP (Calipari et al., 2017).

One limitation of our study is that all experiments were performed in male mice. Given known sex differences in DA function related to cocaine conditioning, and human studies showing females with substance use disorders have more difficulty staying abstinent (Becker and Hu, 2008; Quigley et al., 2021), there may also be sex differences in the influence of ChIN activity on extinction learning.

STAR★METHODS

RESOURCE AVAILABILITY

Lead contact—Further information and requests for resources and reagents should be directed to and will be fulfilled by the lead contact, Ilana B. Witten (iwitten@princeton.edu).

Materials availability—This study did not generate new unique reagents.

Data and code availability

- Neural and behavioral data reported in this paper have been deposited at Figshare and are publicly available as of the date of publication. The DOI is listed in the key resources table.
- All original code has been deposited at Figshare and is publicly available as of the date of publication. The DOI is listed in the key resources table.
- Any additional information required to reanalyze the data reported in this paper is available from the lead contact upon request.

EXPERIMENTAL MODEL AND SUBJECT DETAILS

For plasticity experiments, ChAT::IRES-Cre mice (JAX stock 006410: B6.129S6-Chattm2(cre)Lowl/J [RRID: IMSR_JAX:006410]) were maintained on a C57/BL6J background. We used male mice resulting from the cross of ChAT::IRES-Cre mice and Drd1a-tdTomato mice (JAX stock 016204: B6.Cg-Tg(Drd1a-tdTomato)6Calak/J [RRID: IMSR_JAX:016204]). We also used male mice resulting from the cross of ChAT::IRES-Cre mice and Drd2-EGFP mice (MMRRC stock 000230-UNC: STOCK Tg(Drd2-EGFP)S118Gsat/Mmnc [RRID: MMRRC_000230-UNC]). To ensure these mice were on a C57/BL6J background, Drd2-EGFP had been backcrossed with C57/BL6J mice for at least four generations.

To measure acetylcholine biosensor fluorescence in NAc medial shell, we used ChAT::IRES-Cre mice from the above breedings that either did not express a BAC transgene for fluorophore expression or expressed Drd1a-tdTomato.

Mice were of ages 9–20 weeks. Mice were group-housed with 2–5 mice/cage on a 12-h on, 12-h off light schedule. Only male mice were used. For notes on limitations of the study related to sex, see “Limitations of the study“ in the Discussion. All behavioral testing was performed during the light off time. All experimental and surgical protocols were approved by Princeton University IACUC to meet guidelines of the NIH guide for the Care and Use of Laboratory Animals.

METHOD DETAILS

Cocaine conditioned place preference—On the first day, each mouse was placed on the left side of the CPP chamber and allowed to freely explore the entire apparatus for 15 min (pre-test). The CPP chamber (50 cm × 25 cm, acrylic, California Model & Design Group) consisted of two equally sized compartments (25 cm × 25 cm). Each compartment contained a distinct floor grating (consisting of 4 mm diameter metal rods arranged either in a "mesh" pattern with 10 mm of space between rods or in a line pattern with 10 mm of space between rods) and wall pattern (alternating black and white stripes, 2.5 cm wide, arranged either vertically or horizontally) to allow for compartments to have discriminative visual and tactile cues. Cocaine conditioning followed a counterbalanced design, where the cocaine side was not determined based on the animal's baseline preference. An unbiased apparatus was used. During conditioning, an opaque partition separated CPP compartments. Conditioning occurred on days 2 and 3. On each conditioning day, each mouse was confined to one of the side chambers for approximately 18–20 min in the morning and then to the opposite chamber in the afternoon for the same period of time. Before placement into a given chamber, intraperitoneal injections of cocaine (15 mg/kg; Sigma-Aldrich) before placement in one chamber or intraperitoneal injections of an equal volume of saline (~0.1 mL) before being placed in the other chamber. On day 4, extinction testing began. On this day, mice were allowed to again freely explore the entire apparatus for 15 min.

For the repeat extinction experiment (Figure 1), one group of mice underwent an extinction test each day from days 4–7. For the experiments in Figures 1, 2, and 3, no injections were given prior to these tests. Immediately following the final extinction test, mice were killed for *ex vivo* electrophysiology. Another group of mice underwent conditioning, but never returned to the behavior room after their final conditioning session. These mice were also killed on day 7 for *ex vivo* electrophysiology at approximately the same time of day as mice who underwent repeat extinction testing (1200 h).

For the chemogenetic ChIN inhibition experiment (Figure 4), mice underwent extinction tests each day from days 4–7. Injections of clozapine N-oxide (CNO dihydrochloride; 3 mg/kg, i.p.; HelloBio) were given 30 min before each test. Mice were killed on day 7 for *ex vivo* electrophysiology immediately following the final extinction test on day 7. See Chemogenetic inhibition of cholinergic interneurons for additional details.

For the acetylcholine sensor experiment (Figures 2 and 3), before each session, mice were connected to the photometry patch cable and placed in their home cage for 10 min. After the session, mice were returned to their home cage for 5 min. Mice remained plugged into the patch cable during injections for conditioning sessions.

For the optogenetic experiment (Figure 5), on the day 1 Baseline session, mice were connected to patch cables that were not emitting light. On the day 4 extinction test, mice were again connected to the patch cables. Experimental mice received optogenetic stimulation during the 15 min extinction test. All mice were killed immediately afterward for *ex vivo* electrophysiology. See Optogenetic stimulation of cholinergic interneurons for additional details.

Recordings of acetylcholine biosensor fluorescence—Mice were injected unilaterally or bilaterally with 600 nL of AAV2/9-hSyn-GACh3.0-WPRE-hGHpA (Jing et al., 2020) (PNI Viral Core Facility, injected titer of $6.5*10^{13}$ genome copies/mL) in the ventral-medial NAc at each of two sites (M-L, 0.65 mm; A-P, 1.43 mm; D-V, 4.75 mm) and (M-L, 0.65 mm; A-P, 1.43 mm; D-V, 4.55 mm). Optical fibers (400 μm core diameter, 0.48 NA) were implanted unilaterally or bilaterally at a 10° angle to target the injection region in the NAc (non-rotated coordinates: M-L, 0.685 mm; A-P, 1.43 mm; D-V, 4.55 mm; rotated coordinates at 10°: M-L, 1.46 mm; A-P, 1.43 mm; D-V, 4.36 mm).

To record neural activity with GACh3.0 expressed non-specifically in NAc, mice were connected to a fiber photometry setup (Cai et al., 2020; Parker et al., 2016). In all cases, recordings were unilateral from the same site in a given mouse; in bilaterally surgerized mice, the recording site was selected based on the apparent quality of the fluorescence signal at least one day before behavior testing. Light from the excitation laser (488 nm; Micron Technology) was filtered (FL488, Thorlabs) then passed through a dichroic mirror (MD498, Thorlabs) and traveled through a patch cable (Mono Fiber-optic Patchcord, 400 μm core, 0.48 NA, Doric Lenses) coupled via ceramic split sleeve (2.5 mm diameter, Precision Fiber Products) to the optic fiber implanted in the mouse brain. Laser light delivery was controlled by a lock-in amplifier (Ametek, 7265 Dual Phase DSP Lock-in Amplifier), which delivered light at 210.999 Hz, and the light intensity at the tip of the patch cable was approximately 20 μW. Fluorescent emission from GACh3.0 was then passed through the same patch cable, filtered (MF525–39, Thorlabs), and passed through the same dichroic mirror into a photodetector (Model 2151, New Focus), and the signal was acquired using the same-lock-in amplifier, with a time constant of 20 ms. AC gain on the lock-in amplifier was set to 0 dB. Signal was digitized at 100 Hz on a data acquisition board (USB-201, Measurement Computing) and stored.

dF/F was calculated by the following formula:

$$dF/F(t) = (F(t) - F_0(t))/F_0(t)$$

Where $F_0(t)$ is an estimate of the baseline fluorescence at time t. To isolate transient events and discard slower fluctuations in the signal, $F_0(t)$ was calculated as the fifth percentile based on the preceding 5 s of the recording. Z-score of dF/F signal was calculated across experiment days for each mouse; the mean and standard deviation used for Z-score were the mean and standard deviation of the concatenated dF/F signal across all behavioral sessions from all 7 experiment days.

For event detection from the DF/F, for each mouse, we determined a threshold amplitude that local maxima in the z-scored trace must surpass. To calculate this threshold, we used a heuristic on the data after omitting large peaks. To omit large peaks, we first calculated an initial threshold which was set to 2 * the mean absolute deviation (MAD) above the median of the z-scored trace. We used the MATLAB function “findpeaks” to find peaks with amplitudes that exceeded this initial threshold, and omit indices +/− half of the width at half max. The threshold for peak detection was set to 2*MAD above the median of the trace with large peaks excluded. Peak detection was then performed on the original z-scored traces

using the MATLAB function “findpeaks” with the minimum peak height set to the threshold, and a minimum inter-peak-interval of 100 ms, meaning that if there were multiple events within 100 ms, only the 1st was recorded.

Chemogenetic inhibition of cholinergic interneurons—During surgery, AAV5-hSyn-DIO-hM4D(Gi)-mCherry (Princeton Viral Core, injected 1 uL per hemisphere at a titer of 3.0×10^{13} genome copies/mL) was infused bilaterally in ventral medial NAc (M-L, +/− 0.65 mm; A-P, 1.43 mm; D-V, 4.75 mm) of experimental mice. Control mice received bilateral infusions of AAV2-EF1a-DIO-mCherry (Princeton Viral Core, injected 1 uL per hemisphere at a titer of 3.8×10^{13} genome copies/mL) at the same coordinates in ventral medial NAc. Animals were anesthetized for surgeries with isofluorane (3–4% induction and 1–2% maintenance). Behavioral testing occurred 3–4 weeks after surgery to allow for animal recovery and viral expression. During a repeat extinction cocaine CPP behavior experiment (see Cocaine conditioned place preference), both experimental and control mice received injections of clozapine *N*-oxide (CNO dihydrochloride; 3 mg/kg, i.p.; HelloBio) 30 min before each Test session.

Optogenetic stimulation of cholinergic interneurons—During surgery, AAV5-EFIa-DIO-ChR2-eYFP (PNI Viral Core, injected 1 uL per hemisphere at titer of 1.2×10^{14} genome copies/mL) was infused bilaterally in ventral medial NAc (M-L, +/− 0.65 mm; A-P, 1.43 mm; D-V, 4.75 mm). Optic fibers (300 mm core diameter, 0.37 NA) delivering 10 mW of 447 nm laser light (measured at the end of the patch cable) were implanted bilaterally at a 10° angle to target the ventral medial NAc (non-rotated coordinates: M-L, +/− 0.77 mm; A-P, 1.43 mm; D-V, −4.45 mm; rotated coordinates at 10°: M-L, +/− 1.55 mm; A-P, 1.43 mm; D-V, −4.25 mm). Animals were anesthetized for implant surgeries with isoflurane (3–4% induction and 1–2% maintenance). Behavioral testing occurred 3–4 weeks after surgery to allow for animal recovery and viral expression. Mice were plugged into the patch cables during the baseline and the extinction test sessions. In experimental animals, during extinction testing, light was administered throughout the test in a burst pattern with 5 ms wide pulses at 15 Hz for 2s interleaved with 2s light off periods. We chose these optogenetic stimulation parameters because of their established behavioral and synaptic plasticity effects (Lee et al., 2016), and with the ultimate aim of increasing the rate of synchronous activity among ChINs. Control animals received the same surgery and were plugged into the same patch cable, but no light was administered during extinction testing.

***Ex vivo* electrophysiology—**All electrophysiology experiments were performed on brain slices collected at approximately the same time of day. Mice were anesthetized with an i.p. injection of Euthasol (0.06 mL/30 g). Mice were decapitated and the brain was extracted. After extraction, the brain was immersed in ice-cold NMDG ACSF (92 mM NMDG, 2.5 mM KCl, 1.25 mM NaH2PO4, 30 mM NaHCO3, 20 mM HEPES, 25 mM glucose, 2 mM thiourea, 5 mM Na-ascorbate, 3 mM Na-pyruvate, 0.5 mM CaCl2·4H2O, 10 mM MgSO4·7H2O, and 12 mM N-Acetyl-L-cysteine; pH adjusted to 7.3–7.4) for 2 min. Afterwards coronal slices (300 μm) were sectioned using a vibratome (VT1200s, Leica, Germany) and then incubated in NMDG ACSF at 34 C for approximately 14 min. Slices were then transferred into a holding solution of HEPES ACSF (92 mM NaCl, 2.5 mM KCl,

1.25 mM NaH2PO4, 30 mM NaHCO3, 20 mM HEPES, 25 mM glucose, 2 mM thiourea, 5 mM Na-ascorbate, 3 mM Na-pyruvate, 2 mM CaCl2·4H2O, 2 mM MgSO4·7H2O and 12 mM N-Acetyl-l-cysteine, bubbled at room temperature with 95% O2/5% CO2) for at least 45 min until recordings were performed.

Whole-cell recordings were performed using a Multiclamp 700B (Molecular Devices, Sunnyvale, CA) using pipettes with a resistance of 4–7 MOhm filled with an internal solution containing 100 mM cesium gluconate, 0.6 mM EGTA, 10 mM HEPES, 5 mM NaCl, 20m MTEA, 4mM Mg- ATP, 0.3 mM Na-GTP and 3 mM QX 314 with the pH adjusted to 7.2 with CsOH and the osmolarity adjusted to around 289 mmol kg–1 with sucrose. During recordings, slices were perfused with a recording ACSF solution (120 mM NaCl, 3.5 mM KCl, 1.25 mM NaH2PO4, 26 mM NaHCO3, 1.3 mM MgCl2, 2 mM CaCl2 and 11 mM D-(+)-glucose) that was continuously bubbled with 95% O2/5% CO2. Infrared differential interference contrast–enhanced visual guidance was used to select neurons that were 3–4 cell layers below the surface of the slices. MSNs were identified by the presence of either eGFP or td-Tomato of BAC transgenic mice using a fluorescence microscope (Scientifica SliceScope Pro 1000; LED: SPECTRA X light engine (Lumencor)). The recording solution was delivered to slices via superfusion driven by peristaltic pump (flow rate of 4–5 mL/min) and was held at room temperature. The neurons were held at −70 mV (voltage clamp), and the pipette series resistance was monitored throughout the experiments by hyperpolarizing steps of −10 mV with each sweep. If the series resistance changed by >20% during the recording, the data were discarded. Whole-cell currents were filtered at 1 kHz and digitized and stored at 10 KHz (Clampex 10; MDS Analytical Technologies). All experiments were completed within 4 h after slices were made to maximize cell viability and consistency.

Miniature EPSCs (mEPSCs) were recorded in the presence of TTX (1 μM), d-AP5 (50 μM) and picrotoxin (100 μM) in the recording ACSF solution. mEPSC data was analyzed with Stimfit (Guzman et al., 2014) using detection threshold of >7 pA and rise time <3 ms, and the results were visually verified. For each cell, a stretch of 300 mEPSCs were analyzed, with data collection beginning 10–15 min after patching onto each cell.

For paired pulse ratio (PPR) and AMPA/NMDA ratio measurements, picrotoxin (100 μM) was added to the recording ACSF solution. A bipolar stimulating electrode was placed at the medial-ventral edge of the NAc (see Figure S6 for example electrode placement). For PPR, every 30 s, a paired-pulse stimulation was delivered with a 50 ms inter-stimulus interval (ISI). Stimulation duration was 0.1 ms and current was approximately 0.02–0.08 mA. Evoked EPSCs were recorded from MSNs at a holding potential of −70 mV. 10 repetitions of the stimulation protocol were recorded per cell after stable evoked EPSCs were achieved. PPR was calculated as the ratio between the peak amplitudes of the second and first EPSC. To determine AMPA receptor and NMDA receptor currents, evoked EPSCs were recorded from MSNs at a holding potential of +40 mV. After approximately 10 stimulations, d-AP5 (50 μM) was bath applied to block NMDA receptor currents and isolate AMPA receptor currents. At least 10 evoked EPSCs were recorded following bath application of dAP-5. The NMDA receptor current was calculated as the difference of the mean currents in the absence and presence of d-AP5. In example traces, stimulation artifacts have been removed.

For temporal summation and intrinsic excitability experiments, pipettes were filled with a potassium-based internal solution containing 120 mM potassium gluconate, 0.2 mM EGTA, 10 mM HEPES, 5 mM NaCl, 1 mM MgCl2, 2 mM Mg-ATP and 0.3 mM NA-GTP, with the pH adjusted to 7.2 with KOH.

For the temporal summation experiment, the internal solution also contained 50 μM Alexa Fluor 594 hydrazide for visualization of dendrites. EPSP-like depolarizations mediated by activation of AMPA receptors were evoked using short iontophoretic pulses (10 pulses at 20 Hz with duration 3 ms at 200 nA) of sodium glutamate (150 mM) (Müller and Remy, 2013; Shen et al., 2007) from a puff pipette (pipette resistance 30 MOhm) to a region of visibly identified dendrite approximately 50–100 μm from the soma. Sodium glutamate solution also contained 50 μM Alexa Fluor 594 hydrazide for visualization of puff pipette tip and confirmation of release. Experiments were performed with TTX (1 μM), d-AP5 (50 μM) and picrotoxin (100 μM) in the recording ACSF solution.

For intrinsic excitability experiments, current-clamp recordings were performed in which the resting membrane potential was normalized to −80 mV. In some cases, the resting membrane potential was brought to −80 mV by small current injections of <50 pA. If the compensating current was >50 pA, the recording of the neuron was terminated (Mu et al., 2010). To measure evoked spiking, a current step protocol (−200 to +350 pA; 50 pA increment; 15 s interpulse interval) was run for 5 runs (Mu et al., 2010).

***Ex vivo* confirmation of ACh sensor response selectivity—**To confirm that tissue expressing GACh3.0 was responsive to acetylcholine but not cocaine, mice were injected bilaterally with 600 nL of AAV 2/9 with hSyn-GACh3.0-WPRE-hGHpA (PNI Viral Core Facility, injected titer of $6.5*10^{13}$ genome copies/mL) in the ventral-medial NAc in two sites (M-L, 0.65 mm; A-P, 1.43 mm; D-V, 4.75 mm) and (M-L, 0.65 mm; A-P, 1.43 mm; D-V, 4.55 mm). 3 weeks after surgery, we performed *ex vivo* slice imaging. Brain slices were collected using the methods and solutions described in *Ex vivo* electrophysiology. During recordings, slices were perfused with the recording ACSF solution (see *Ex vivo* electrophysiology). Fluorescence was imaged using a CMOS camera (ORCA-Flash 2.8, Hamamatsu) at 33.333 Hz (30 ms exposure windows) using a GFP filter cube set (excited ET470/40x, dichroic T495LP, emitter ET525/50m) (Fleming et al., 2021). To test for fluorescence responses to acetylcholine or cocaine, a glass pipette filled with recording ACSF containing a given drug (100 μM acetylcholine, 10 μM cocaine, or 100 μM cocaine) was placed above a segment of tissue. Slight positive pressure (approximately 80 kPa) was briefly applied (100 ms), and time-locked fluorescence responses were recorded. Recordings were performed on the same segment of tissue, but for each drug the pipette was replaced and repositioned over the tissue.

Immunohistochemistry: Mice were first anesthetized and then transcardially perfused with cold 4% paraformaldehyde (PFA) in PBS (pH 7.4). Brains were fixed in 4% PFA. 50 μm coronal slices were sectioned on a vibratome, and then were subsequently stored in cryoprotectant at 4°C. For immunohistochemistry, individual sections were washed in PBS and then incubated for 30 min in 0.3% Triton-X and 3% normal donkey serum (NDS).

For ChAT labeling (Figure S6), ChAT primary antibody (1:200; Millipore, Product# AB144P [RRID: AB_2079751]) incubations were performed overnight at 4°C in 3% NDS/PBS. Sections were washed and left to incubate in secondary antibodies conjugated to AlexaFluor586 for 3 h at room temperature (1:1000; Invitrogen, Product#A-11004 [RRID: AB_10564097]).

For enhancement of GFP in GACh3.0 tissue labeling (Figure 2B), GFP primary antibody (1:500; Millipore, product # NB600-308 [RRID: AB_10003058]) incubations were performed overnight at 4°C in 3% NDS/PBS. Sections were washed and left to incubate in secondary antibodies conjugated to AlexaFluor586 for 3 h at room temperature (1:1000; Invitrogen, Product#A-11004 [RRID: AB_10564097]).

Following a 20 min incubation with DAPI (1:50,000) sections were washed and mounted on microscope slides with Fluorogold (Southern Biotechnology, product # 0100-01).

In situ *RNA hybridization*: For the *in situ* RNA hybridization experiments (Figure S1), mice were anesthetized with 0.1 mL Euthasol (i.p. injection) and transcardially perfused with 4% PFA in PBS. Brains were dissected out and post-fixed in 4% PFA overnight. Brains were then put through a sucrose gradient: 10% sucrose in PBS solution for 6–8 h, 20% sucrose in PBS solution overnight, and then 30% sucrose in PBS solution overnight. 18 μm thick coronal sections containing the nucleus accumbens were cut on a cryostat. *In situ* hybridization was performed on mounted sections using the RNAscope Multiplex Fluorescent Assay (Advanced Cell Diagnostics, Inc., No. 323110). Custom probes were used for Mm-Drd1a-C1 (406491-C1) and Mm-Drd2-C2 (406501-C2; 1:50 dilution in C1 probe solution), and Mm-tdTomato-C3 (317041-C3, 1:50 dilution in C1 probe solution for drd1a-tdTomato mice only). The following fluorophores (Perkin Elmer, NEL760001KT) were used to report RNA detection in each channel: fluorescein (C2 in drd1a-tdTomato slices), cy3 (C3 in drd1a-tdTomato slices; C1 in drd2-eGFP slices), and cy5 (C1 in drd1a-tdTomato slices; C2 in drd2-eGFP slices). Fluorophores were reconstituted in 60 mL DMSO and diluted in TSA buffer provided in the RNAscope kit at a concentration of 1:1200. Following the *in situ* hybridization protocol, a GFP antibody stain was used to enhance visualization of drd2-eGFP expression. The primary antibody was a mouse monoclonal anti-GFP (1:1000 dilution, Life Technologies, No. G10362; RRID: AB_2536526) and the secondary was a donkey anti-rabbit coupled to Alexa 488 (1:1000 dilution, Jackson ImmunoResearch, No. 711-545-152). Cellular resolution images of mounted coronal sections were acquired using a Zeiss confocal microscope (LSM 700; four visible solid-state lasers: UV 405; argon 458/488; HeNe 555/568; far-red 639) (Oberkochen, Germany). The first example image in Figure 2A was taken at 63x, 0.7x zoom with oil immersion, and the second image was taken at 63x, 2.0x zoom with oil immersion.

QUANTIFICATION AND STATISTICAL ANALYSIS

Behavioral preference for repeat extinction CPP experiments with only one experimental group undergoing repeat preference (Figures 1B and S4) was assessed using the “aov” function in R to perform a one-way repeated measures ANOVA with session as fixed effect and mouse as random effect. Post-hoc tests comparing Baseline to Test 1 preference were

performed using the “pairwise.t.test” function in R to perform a pairwise t test between preference during the two sessions with Holm’s adjustment for multiple comparisons.

To compare changes in ACh event frequency in Figures 2F and 2G, we used pairwise t-tests, using the “ttest” function in MATLAB, of mean event frequency between Baseline and Test 1 for the 10 min period before behavior, the 15 min behavioral period, and the 5 min period after behavior. To compare event frequency based on chamber side, pairwise t-tests were performed using the mean frequencies for each mouse on the saline vs cocaine zone. To measure the relationship between event frequency on Test 1 and preference on Tests 1–4 (Figures 2J and S4), we calculated the correlation coefficient and corresponding p values between Test 1 frequency and test preferences using the “corrcoef” function in MATLAB. Additionally, for Figure 2K, we measured the relationship between Test 1 frequency groups and preference on Tests 1–4 with a repeated measures ANOVA using the “aov” function in R, where preference was predicted using median split frequency group, session (Tests 1–4), and their interaction as fixed effects, and mouse as a random effect.

To measure how speed was affected by ACh events (Figures 3B–3D), we calculated the baseline-corrected change in speed around the time of each event. Baseline speed was calculated as mean speed in a 1 s window starting 2 s before the ACh event peak time. The speed around each event was calculated as the mean speed in a 1.5 s window beginning 0.5 s before the time event peak time and ending 1 s after the event peak time. The change in speed was calculated as the difference between the baseline speed and the speed around the time of the event (Figure 3D).

To measure the relationship between speed and event frequency (Figures 3E), 10 speed deciles were first calculated for each mouse using combined speed data from both the Baseline and Test 1 sessions. For each session, the number of events occurring while the animal was moving at a speed within a given decile range was counted and divided by the time the animal spent in that speed range (1/10 of total time between the two behaviors) to calculate event frequencies. Mean event frequencies were calculated for each speed decile for Baseline and Test 1. To quantify the relationship between speed and event frequency, we performed a linear, mixed-effects regression using the “lmer” function in R, with frequency predicted using speed decile, behavioral session, and their interaction as fixed effects, and mouse as a random effect. was calculated by inputting the resulting model into the “lme.dscore” function in the “EMAtools” package in R. To compare how the slope of the speed decile vs. event frequency plots corresponded to preference on Tests 1–4 (Figure 3F), slopes for each mouse were first calculated by fitting the mean event frequency across speed deciles by fitting the data to a linear function using the “polyfit” function in MATLAB. Slopes were median split, and we performed a repeated measures ANOVA using the “aov” function in R, where preference was predicted using the median split group, session (Tests 1–4), and their interaction as fixed effects, and mouse as a random effect.

To compare differences in preference between experimental groups in the chemogentic experiment (Figure 4F), we used a repeated measures ANOVA, using the “aov” function in R, where preference was predicted using experimental group (ChIN inactivation vs control), session (Tests 2–4), and their interaction as fixed effects, and mouse as a random effect.

Additionally, to determine whether session predicted preference within a group, separate one-way repeated measures ANOVAs ("aov" in R) were run for each experimental group (ChIN activation and control), where preference was predicted using session (Tests 1–4) as a fixed effect and mouse as a random effect.

To compare differences in preference between experimental groups in the optogenetic experiment (Figure 5E; Figure S7), we performed a multi-factor, repeated measures ANOVA using the "aov" function in R, where preference was predicted using mouse transgenic line (drd1a-tdTomato or drd2-GFP), group (Control vs ChIN activation), and session (Baseline vs Test), and their interactions as fixed effects, with mouse as a random effect. Two post-hoc t-tests were performed between groups (Control vs ChIN activation) for both Baseline and Test days using the "pairwise.t.test" function in R. To compare differences between groups (Control vs ChIN activation) as a function of time during the Test session (Figure 5F), we first calculated the fraction of time each animal spent in the cocaine zone during the Test, divided into unsmoothed, non-overlapping 1 min bins. With this data, we used the "lmer" function in R to perform a linear, mixed-effects regression on preference for the cocaine zone using group (Control vs ChIN activation), time (min bins 1–15), and their interaction as fixed effects, with mouse as a random effect. We performed a series of post-hoc t-tests using the "pairwise.t.test" function, with Holm's correction, to determine at which time points were the Control and ChIN activation groups different.

To compare the mEPSC frequency and amplitudes across conditions, linear, mixed-effects regressions were performed using the "lmer" function in R. Interevent interval (IEI) data was log-transformed while amplitude data was inverse-transformed to best fit a normal distribution. For statistical analysis of both IEI data and amplitude data for Figures 1E–1H, the linear, mixed effects regression model included group (No extinction vs. Repeat extinction) as a fixed effect and cell as a random effect. For statistical analysis of both IEI data and amplitude data for Figures 4I–4L and 5H–5K, the linear, mixed effects regression model included group (Control vs. Experimental (either ChIN inhibition or activation)) as a fixed effect and cell as a random effect. Effect sizes were calculated as Cohen's d using the "lme.dscore" function in the "EMATools" package in R. Separate regressions were calculated for data from D1R and D2R MSNs.

To compare differences in paired pulse ratio and AMPA/NMDA ratio between groups (Control vs Experimental; Figures 1J, 1K and 5L–5Q), we performed two-tailed t-tests using the "ttest2" function in MATLAB. Effect sizes were calculated as Cohen's d using custom written software in MATLAB, where the difference in means between the two datasets is divided by the pooled standard deviations of the two datasets. Separate analyses were calculated for data from D1R and D2R MSNs.

To compare the difference in temporal summation of excitatory EPSPs in the glutamate iontophoresis experiment (Figures 5R and 5S), for each recording all EPSPs were first normalized to the amplitude of the first EPSP in the respective trace. We compared the amplitudes of these normalized EPSPs between groups (Control vs ChIN activation) by using the "lmer" function in R to perform a linear, mixed effects regression on EPSP

amplitude using group, EPSP number, and their interaction as another fixed effect, with cell as a random effect.

To compare the differences in evoked spikes as a function of injected current between groups (Figure 5U), we first calculated the mean number of spikes for each current step across all runs for a given cell. If the mean number of spikes decreased with increasing current injection (because of depolarization block), data from that current step and above was removed. Separately for D1R and D2R MSN data, we used the “lmer” function in R to perform a linear, mixed-effects regression on the number of evoked spikes, using group (Control vs ChIN activation), injected current value, and their interaction as fixed effects, with cell as a random effect. We also inputted the resulting model into R function “testInteractions” to determine whether the slopes of the current vs. evoked spikes lines were significantly different between groups (Control vs ChIN activation). Effect sizes were calculated using the “lme.dscore” function in the “EMAtools” package in R.

For action potential statistics in the evoked spiking experiment (Figures 5T and 5U; Figure S7), only the first spike in each run was used. Action potential threshold was calculated as the first point of positive acceleration of voltage ($(\Delta V/\Delta t)/\Delta t$) that exceeded 3*SD of membrane noise in the period prior to current injection (Baufreton et al., 2005; Willett et al., 2019). The fast afterhyperpolarization potential was calculated as the voltage value 8 ms following onset of the first actional potential in a run; the medium afterhyperpolarization potential was calculated as the voltage 16 ms following the onset of the first action potential.

Supplementary Material

Refer to Web version on PubMed Central for supplementary material.

ACKNOWLEDGMENTS

We thank V. Corbit, A. Pan-Vazquez, and N.F. Parker for comments on the manuscript, as well as other members of the Witten laboratory for their support. We thank B. Juarez for discussion on individual differences in neuromodulation. We thank E. Engel and the PNI Viral Core for reagents. This work was supported by grants from NSF GRFP (W.F., B.A.B.), F32 MH118792 (S.S.B.), NIH R01 DA047869 (I.B.W.), U19 NS104648-01 (I.B.W.), ARO W911NF1710554 (I.B.W.), Brain Research Foundation (I.B.W.), Simons Collaboration on the Global Brain (I.B.W.), and the New York Stem Cell Foundation (I.B.W.). I.B.W. is an NYSCF-Robertson Investigator.

REFERENCES

Aitta-Aho T, Phillips BU, Pappa E, Hay YA, Harnischfeger F, Heath CJ, Saksida LM, Bussey TJ, and Apergis-Schoute J (2017). Accumbal cholinergic interneurons differentially influence motivation related to satiety signaling. eNeuro 4. 10.1523/eneuro.0328-16.2017.

Al-Hasani R, Gowrishankar R, Schmitz GP, Pedersen CE, Marcus DJ, Shirley SE, Hobbs TE, Elerding AJ, Renaud SJ, Jing M, et al. (2021). Ventral tegmental area GABAergic inhibition of cholinergic interneurons in the ventral nucleus accumbens shell promotes reward reinforcement. Nat. Neurosci 24, 1414–1428. [PubMed: 34385700]

Aosaki T, Graybiel AM, and Kimura M (1994). Effect of the nigrostriatal dopamine system on acquired neural responses in the striatum of behaving monkeys. Science 265, 412–415. 10.1126/science.8023166. [PubMed: 8023166]

Apicella P (2017). The role of the intrinsic cholinergic system of the striatum: what have we learned from TAN recordings in behaving animals? Neuroscience 360, 81–94. 10.1016/j.neuroscience.2017.07.060. [PubMed: 28768155]

Apicella P, Scarnati E, and Schultz W (1991). Tonically discharging neurons of monkey striatum respond to preparatory and rewarding stimuli. Exp. Brain Res 84, 672–675. 10.1007/bf00230981. [PubMed: 1864338]

Armbruster BN, Li X, Pausch MH, Herlitze S, and Roth BL (2007). Evolving the lock to fit the key to create a family of G protein-coupled receptors potently activated by an inert ligand. Proc. Natl. Acad. Sci. U. S. A 104, 5163–5168. 10.1073/pnas.0700293104. [PubMed: 17360345]

Barral J, Galarraga E, and Bargas J (1999). Muscarinic presynaptic inhibition of neostriatal glutamatergic afferents is mediated by Q-type Ca2+ channels. Brain Res. Bull 49, 285–289. 10.1016/s0361-9230(99)00061-1. [PubMed: 10424849]

Baufreton J, Atherton JF, Surmeier DJ, and Bevan MD (2005). Enhancement of excitatory synaptic integration by GABAergic inhibition in the subthalamic nucleus. J. Neurosci 25, 8505–8517. 10.1523/jneurosci.1163-05.2005. [PubMed: 16162932]

Becker JB, and Hu M (2008). Sex differences in drug abuse. Front. Neuroendocrinol 29, 36–47. 10.1016/j.yfrne.2007.07.003. [PubMed: 17904621]

Berlanga ML, Olsen CM, Chen V, Ikegami A, Herring BE, Duvauchelle CL, and Alcantara AA (2003). Cholinergic interneurons of the nucleus accumbens and dorsal striatum are activated by the self-administration of cocaine. Neuroscience 120, 1149–1156. 10.1016/s0306-4522(03)00378-6. [PubMed: 12927219]

Bernard V, Normand E, and Bloch B (1992). Phenotypical characterization of the rat striatal neurons expressing muscarinic receptor genes. J. Neurosci 12, 3591–3600. 10.1523/jneurosci.12-09-03591.1992. [PubMed: 1527598]

Bock R, Shin JH, Kaplan AR, Dobi A, Markey E, Kramer PF, Gremel CM, Christensen CH, Adrover MF, and Alvarez VA (2013). Strengthening the accumbal indirect pathway promotes resilience to compulsive cocaine use. Nat. Neurosci 16, 632–638. 10.1038/nn.3369. [PubMed: 23542690]

Bordia T, Perez XA, Heiss JE, Zhang D, and Quik M (2016). Optogenetic activation of striatal cholinergic interneurons regulates L-dopa-induced dyskinesias. Neurobiol. Dis 91, 47–58. 10.1016/j.nbd.2016.02.019. [PubMed: 26921469]

Boudreau AC (2005). Behavioral sensitization to cocaine is associated with increased AMPA receptor surface expression in the nucleus accumbens. J. Neurosci 25, 9144–9151. 10.1523/jneurosci.2252-05.2005. [PubMed: 16207873]

Boudreau AC, Reimers JM, Milovanovic M, and Wolf ME (2007). Cell surface AMPA receptors in the rat nucleus accumbens increase during cocaine withdrawal but internalize after cocaine challenge in association with altered activation of mitogen-activated protein kinases. J. Neurosci 27, 10621–10635. 10.1523/jneurosci.2163-07.2007. [PubMed: 17898233]

Bouton ME (2004). Context and behavioral processes in extinction: table 1. Learn. Mem 11, 485–494. 10.1101/lm.78804. [PubMed: 15466298]

Britt JP, Benaliouad F, McDevitt RA, Stuber GD, Wise RA, and Bonci A (2012). Synaptic and behavioral profile of multiple glutamatergic inputs to the nucleus accumbens. Neuron 76, 790–803. 10.1016/j.neuron.2012.09.040. [PubMed: 23177963]

Cachope R, Mateo Y, Mathur BN, Irving J, Wang H-L, Morales M, Lovinger DM, and Cheer JF (2012). Selective activation of cholinergic interneurons enhances accumbal phasic dopamine release: setting the tone for reward processing. Cell Rep 2, 33–41. 10.1016/j.celrep.2012.05.011. [PubMed: 22840394]

Cai LX, Pizano K, Gundersen GW, Hayes CL, Fleming WT, Holt S, Cox JM, and Witten IB (2020). Distinct signals in medial and lateral VTA dopamine neurons modulate fear extinction at different times. Elife 9. 10.7554/elife.54936.

Calipari ES, Bagot RC, Purushothaman I, Davidson TJ, Yorgason JT, Peña CJ, Walker DM, Pirpinias ST, Guise KG, Ramakrishnan C, et al. (2016). *In vivo* imaging identifies temporal signature of D1 and D2 medium spiny neurons in cocaine reward. Proc. Natl. Acad. Sci. U. S. A 113, 2726–2731. 10.1073/pnas.1521238113. [PubMed: 26831103]

Calipari ES, Juarez B, Morel C, Walker DM, Cahill ME, Ribeiro E, Roman-Ortiz C, Ramakrishnan C, Deisseroth K, Han M-H, and Nestler EJ (2017). Dopaminergic dynamics underlying sex-specific cocaine reward. Nat. Commun 8, 13877. 10.1038/ncomms13877. [PubMed: 28072417]

Choi S, and Lovinger DM (1997). Decreased probability of neurotransmitter release underlies striatal long-term depression and postnatal development of corticostriatal synapses. Proc. Natl. Acad. Sci. U. S. A 94, 2665–2670. 10.1073/pnas.94.6.2665. [PubMed: 9122253]

Chuhma N, Mingote S, Moore H, and Rayport S (2014). Dopamine neurons control striatal cholinergic neurons via regionally heterogeneous dopamine and glutamate signaling. Neuron 81, 901–912. 10.1016/j.neuron.2013.12.027. [PubMed: 24559678]

Cole SL, Robinson MJF, and Berridge KC (2018). Optogenetic self-stimulation in the nucleus accumbens: D1 reward versus D2 ambivalence. PLoS One 13, e0207694. 10.1371/journal.pone.0207694. [PubMed: 30496206]

Collins AL, Aitken TJ, Huang I-W, Shieh C, Greenfield VY, Monbouquette HG, Ostlund SB, and Wassum KM (2019). Nucleus accumbens cholinergic interneurons oppose cue-motivated behavior. Biol. Psychiatry 86, 388–396. 10.1016/j.biopsych.2019.02.014. [PubMed: 30955842]

Ding JB, Guzman JN, Peterson JD, Goldberg JA, and Surmeier DJ (2010). Thalamic gating of corticostriatal signaling by cholinergic interneurons. Neuron 67, 294–307. 10.1016/j.neuron.2010.06.017. [PubMed: 20670836]

Dorst MC, Tokarska A, Zhou M, Lee K, Stagkourakis S, Broberger C, Masmanidis S, and Silberberg G (2020). Polysynaptic inhibition between striatal cholinergic interneurons shapes their network activity patterns in a dopamine-dependent manner. Nat. Commun 11, 5113. 10.1038/s41467-020-18882-y. [PubMed: 33037215]

Durieux PF, Bearzatto B, Guiducci S, Buch T, Waisman A, Zoli M, Schiffmann SN, and de Kerchove d'Exaerde A (2009). D2R striatopallidal neurons inhibit both locomotor and drug reward processes. Nat. Neurosci 12, 393–395. 10.1038/nn.2286. [PubMed: 19270687]

English DF, Ibanez-Sandoval O, Stark E, Tecuapetla F, Buzsáki G, Deisseroth K, Tepper JM, and Koos T (2011). GABAergic circuits mediate the reinforcement-related signals of striatal cholinergic interneurons. Nat. Neurosci 15, 123–130. 10.1038/nn.2984. [PubMed: 22158514]

Ferrario CR, Loweth JA, Milovanovic M, Ford KA, Galiñanes GL, Heng L-J, Tseng KY, and Wolf ME (2011). Alterations in AMPA receptor subunits and TARPs in the rat nucleus accumbens related to the formation of Ca2+-permeable AMPA receptors during the incubation of cocaine craving. Neuropharmacology 61, 1141–1151. 10.1016/j.neuropharm.2011.01.021. [PubMed: 21276808]

Fleming W, Jewell S, Engelhard B, Witten DM, and Witten IB (2021). Inferring spikes from calcium imaging in dopamine neurons. PLoS One 16, e0252345. 10.1371/journal.pone.0252345. [PubMed: 34086726]

Gallo EF, Meszaros J, Sherman JD, Chohan MO, Teboul E, Choi CS, Moore H, Javitch JA, and Kellendonk C (2018). Accumbens dopamine D2 receptors increase motivation by decreasing inhibitory transmission to the ventral pallidum. Nat. Commun 9, 1086. 10.1038/s41467-018-03272-2. [PubMed: 29540712]

Gerfen CR, Engber TM, Mahan LC, Susel Z, Chase TN, Monsma FJ Jr., and Sibley DR (1990). D1 and D2 dopamine receptor-regulated gene expression of striatonigral and striatopallidal neurons. Science 250, 1429–1432. 10.1126/science.2147780. [PubMed: 2147780]

Ghasemzadeh MB, Mueller C, and Vasudevan P (2009). Behavioral sensitization to cocaine is associated with increased glutamate receptor trafficking to the postsynaptic density after extended withdrawal period. Neuroscience 159, 414–426. 10.1016/j.neuroscience.2008.10.027. [PubMed: 19105975]

Guzman SJ, Schlögl A, and Schmidt-Hieber C (2014). Stimfit: quantifying electrophysiological data with Python. Front. Neuroinform 8, 16. 10.3389/fninf.2014.00016. [PubMed: 24600389]

Hernández-Echeagaray E, Galarraga E, and Bargas J (1998). 3-Alpha-chloro-imperialine, a potent blocker of cholinergic presynaptic modulation of glutamatergic afferents in the rat neostriatum. Neuropharmacology 37, 1493–1502. 10.1016/s0028-3908(98)00131-2. [PubMed: 9886672]

Higley MJ, Soler-Llavina GJ, and Sabatini BL (2009). Cholinergic modulation of multivesicular release regulates striatal synaptic potency and integration. Nat. Neurosci 12, 1121–1128. 10.1038/nn.2368. [PubMed: 19668198]

Hikida T, Kimura K, Wada N, Funabiki K, and Nakanishi S (2010). Distinct roles of synaptic transmission in direct and indirect striatal pathways to reward and aversive behavior. Neuron 66, 896–907. 10.1016/j.neuron.2010.05.011. [PubMed: 20620875]

Howe MW, and Dombeck DA (2016). Rapid signalling in distinct dopaminergic axons during locomotion and reward. Nature 535, 505–510. 10.1038/nature18942. [PubMed: 27398617]

Howe M, Ridouh I, Allegra Mascaro AL, Larios A, Azcorra M, and Dombeck DA (2019). Coordination of rapid cholinergic and dopaminergic signaling in striatum during spontaneous movement. Elife 8. 10.7554/elife.44903.

Iino Y, Sawada T, Yamaguchi K, Tajiri M, Ishii S, Kasai H, and Yagishita S (2020). Dopamine D2 receptors in discrimination learning and spine enlargement. Nature 579, 555–560. 10.1038/s41586-020-2115-1. [PubMed: 32214250]

Jing M, Li Y, Zeng J, Huang P, Skirzewski M, Kljakic O, Peng W, Qian T, Tan K, Zou J, et al. (2020). An optimized acetylcholine sensor for monitoring *in vivo* cholinergic activity. Nat. Methods 17, 1139–1146. 10.1038/s41592-020-0953-2. [PubMed: 32989318]

Joshua M, Adler A, Mitelman R, Vaadia E, and Bergman H (2008). Midbrain dopaminergic neurons and striatal cholinergic interneurons encode the difference between reward and aversive events at different epochs of probabilistic classical conditioning trials. J. Neurosci 28, 11673–11684. 10.1523/jneurosci.3839-08.2008. [PubMed: 18987203]

Juarez B, Morel C, Ku SM, Liu Y, Zhang H, Montgomery S, Gregoire H, Ribeiro E, Crumiller M, Roman-Ortiz C, et al. (2017). Midbrain circuit regulation of individual alcohol drinking behaviors in mice. Nat. Commun 8, 2220. 10.1038/s41467-017-02365-8. [PubMed: 29263389]

Kaneko S, Hikida T, Watanabe D, Ichinose H, Nagatsu T, Kreitman RJ, Pastan I, and Nakanishi S (2000). Synaptic integration mediated by striatal cholinergic interneurons in basal ganglia function. Science 289, 633–637. 10.1126/science.289.5479.633. [PubMed: 10915629]

Kondabolu K, Roberts EA, Bucklin M, McCarthy MM, Kopell N, and Han X (2016). Striatal cholinergic interneurons generate beta and gamma oscillations in the corticostriatal circuit and produce motor deficits. Proc. Natl. Acad. Sci. U. S. A 113, E3159–E3168. 10.1073/pnas.1605658113. [PubMed: 27185924]

Kourrich S, Rothwell PE, Klug JR, and Thomas MJ (2007). Cocaine experience controls bidirectional synaptic plasticity in the nucleus accumbens. J. Neurosci 27, 7921–7928. 10.1523/jneurosci.1859-07.2007. [PubMed: 17652583]

Kravitz AV, Tye LD, and Kreitzer AC (2012). Distinct roles for direct and indirect pathway striatal neurons in reinforcement. Nat. Neurosci 15, 816–818. 10.1038/nn.3100. [PubMed: 22544310]

Laverne G, Pesce J, Reynders A, Melon C, Goff LK-L, Maurice N, and Beurrier C (2021). Inhibition of cholinergic interneurons potentiates corticostriatal transmission in D1 receptor-expressing medium-sized spiny neurons and restores motor learning in parkinsonian condition. Preprint at bioRxiv. 10.1101/2021.07.07.451477.

Lee J, Finkelstein J, Choi JY, and Witten IB (2016). Linking cholinergic interneurons, synaptic plasticity, and behavior during the extinction of a cocaine-context association. Neuron 90, 1071–1085. 10.1016/j.neuron.2016.05.001. [PubMed: 27210555]

Lee JH, Ribeiro EA, Kim J, Ko B, Kronman H, Jeong YH, Kim JK, Janak PH, Nestler EJ, Koo JW, et al. (2020). Dopaminergic regulation of nucleus accumbens cholinergic interneurons demarcates susceptibility to cocaine addiction. Biol. Psychiatry 88, 746–757. 10.1016/j.biopsych.2020.05.003. [PubMed: 32622465]

Lee SJ, Lodder B, Chen Y, Patriarchi T, Tian L, and Sabatini BL (2021). Cell-type-specific asynchronous modulation of PKA by dopamine in learning. Nature 590, 451–456. 10.1038/s41586-020-03050-5. [PubMed: 33361810]

Lewis RG, Serra M, Radl D, Gori M, Tran C, Michalak SE, Vanderwal CD, and Borrelli E (2020). Dopaminergic control of striatal cholinergic interneurons underlies cocaine-induced psychostimulation. Cell Rep 31, 107527. 10.1016/j.celrep.2020.107527. [PubMed: 32320647]

Lim SAO, Kang UJ, and McGehee DS (2014). Striatal cholinergic interneuron regulation and circuit effects. Front. Synaptic Neurosci 6, 22. 10.3389/fnsyn.2014.00022. [PubMed: 25374536]

Lobo MK, Covington HE 3rd, Chaudhury D, Friedman AK, Sun H, Damez-Werno D, Dietz DM, Zaman S, Koo JW, Kennedy PJ, et al. (2010). Cell type-specific loss of BDNF signaling mimics optogenetic control of cocaine reward. Science 330, 385–390. 10.1126/science.1188472. [PubMed: 20947769]

MacAskill AF, Cassel JM, and Carter AG (2014). Cocaine exposure reorganizes cell type– and input-specific connectivity in the nucleus accumbens. Nat. Neurosci 17, 1198–1207. 10.1038/nn.3783. [PubMed: 25108911]

Malenka RC, and Kocsis JD (1988). Presynaptic actions of carbachol and adenosine on corticostriatal synaptic transmission studied *in vitro*. J. Neurosci 8, 3750–3756. 10.1523/jneurosci.08-10-03750.1988. [PubMed: 2848109]

Maurice N, Liberge M, Jaouen F, Ztaou S, Hanini M, Camon J, Deisseroth K, Amalric M, Kerkerian-Le Goff L, and Beurrier C (2015). Striatal cholinergic interneurons control motor behavior and basal ganglia function in experimental parkinsonism. Cell Rep 13, 657–666. 10.1016/j.celrep.2015.09.034. [PubMed: 26489458]

Morris G, Arkadir D, Nevet A, Vaadia E, and Bergman H (2004). Coincident but distinct messages of midbrain dopamine and striatal tonically active neurons. Neuron 43, 133–143. 10.1016/j.neuron.2004.06.012. [PubMed: 15233923]

Mu P, Moyer JT, Ishikawa M, Zhang Y, Panksepp J, Sorg BA, Schlüter OM, and Dong Y (2010). Exposure to cocaine dynamically regulates the intrinsic membrane excitability of nucleus accumbens neurons. J. Neurosci 30, 3689–3699. 10.1523/jneurosci.4063-09.2010. [PubMed: 20220002]

Müller C, and Remy S (2013). Fast micro-iontophoresis of glutamate and GABA: a useful tool to investigate synaptic integration. J. Vis. Exp 77, e50701. 10.3791/50701.

O'Neal TJ, Nooney MN, Thien K, and Ferguson SM (2020). Chemogenetic modulation of accumbens direct or indirect pathways bidirectionally alters reinstatement of heroin-seeking in high- but not low-risk rats. Neuropsychopharmacology 45, 1251–1262. 10.1038/s41386-019-0571-9. [PubMed: 31747681]

Pakhotin P, and Bracci E (2007). Cholinergic interneurons control the excitatory input to the striatum. J. Neurosci 27, 391–400. 10.1523/jneurosci.3709-06.2007. [PubMed: 17215400]

Parker NF, Cameron CM, Taliaferro JP, Lee J, Choi JY, Davidson TJ, Daw ND, and Witten IB (2016). Reward and choice encoding in terminals of midbrain dopamine neurons depends on striatal target. Nat. Neurosci 19, 845–854. 10.1038/nn.4287. [PubMed: 27110917]

Pascoli V, Terrier J, Espallergues J, Valjent E, O'Connor EC, and Lüscher C (2014). Contrasting forms of cocaine-evoked plasticity control components of relapse. Nature 509, 459–464. 10.1038/nature13257. [PubMed: 24848058]

Pavlov IP (1960). Conditioned reflexes: an investigation of the physiological activity of the cerebral cortex (Unabriged and unaltered republication of the translation 1927). Ann. Neurosci 17, 136–141.

Phillipson OT, and Griffiths AC (1985). The topographic order of inputs to nucleus accumbens in the rat. Neuroscience 16, 275–296. 10.1016/0306-4522(85)90002-8. [PubMed: 4080159]

Quigley JA, Logsdon MK, Turner CA, Gonzalez IL, Leonardo NB, and Becker JB (2021). Sex differences in vulnerability to addiction. Neuropharmacology 187, 108491. 10.1016/j.neuropharm.2021.108491. [PubMed: 33567305]

Quirk GJ, and Mueller D (2008). Neural mechanisms of extinction learning and retrieval. Neuropsychopharmacology 33, 56–72. 10.1038/sj.npp.1301555. [PubMed: 17882236]

Rescorla RA (2001). Experimental extinction. Handbook Contemp. Learn. Theories 55, 119–154.

Robbins SJ (1990). Mechanisms underlying spontaneous recovery in autoshaping. J. Exp. Psychol. Anim. Behav. Process 16, 235–249. 10.1037/0097-7403.16.3.235.

Robinson TE, Gorny G, Mitton E, and Kolb B (2001). Cocaine self-administration alters the morphology of dendrites and dendritic spines in the nucleus accumbens and neocortex. Synapse 39, 257–266. 10.1002/1098-2396(20010301)39:3<257::aid-syn1007>3.0.co;2-1. [PubMed: 11169774]

Shen W, Tian X, Day M, Ulrich S, Tkatch T, Nathanson NM, and Surmeier DJ (2007). Cholinergic modulation of Kir2 channels selectively elevates dendritic excitability in striatopallidal neurons. Nat. Neurosci 10, 1458–1466. 10.1038/nn1972. [PubMed: 17906621]

Shen W, Flajolet M, Greengard P, and Surmeier DJ (2008). Dichotomous dopaminergic control of striatal synaptic plasticity. Science 321, 848–851. 10.1126/science.1160575. [PubMed: 18687967]

Sjulson L, Peyrache A, Cumpelik A, Cassataro D, and Buzsáki G (2018). Cocaine place conditioning strengthens location-specific hippocampal coupling to the nucleus accumbens. Neuron 98, 926–934.e5, e5. 10.1016/j.neuron.2018.04.015. [PubMed: 29754750]

Sugita S, Uchimura N, Jiang ZG, and North RA (1991). Distinct muscarinic receptors inhibit release of gamma-aminobutyric acid and excitatory amino acids in mammalian brain. Proc. Natl. Acad. Sci. U. S. A 88, 2608–2611. 10.1073/pnas.88.6.2608. [PubMed: 1672454]

Tang KC, Low MJ, Grandy DK, and Lovinger DM (2001). Dopamine-dependent synaptic plasticity in striatum during *in vivo* development. Proc. Natl. Acad. Sci. U. S. A 98, 1255–1260. 10.1073/pnas.98.3.1255. [PubMed: 11158626]

Thomas MJ, Beurrier C, Bonci A, and Malenka RC (2001). Long-term depression in the nucleus accumbens: a neural correlate of behavioral sensitization to cocaine. Nat. Neurosci 4, 1217–1223. 10.1038/nn757. [PubMed: 11694884]

Thomas MJ, Kalivas PW, and Shaham Y (2008). Neuroplasticity in the mesolimbic dopamine system and cocaine addiction. Br. J. Pharmacol 154, 327–342. 10.1038/bjp.2008.77. [PubMed: 18345022]

Threlfell S, Lalic T, Platt NJ, Jennings KA, Deisseroth K, and Cragg SJ (2012). Striatal dopamine release is triggered by synchronized activity in cholinergic interneurons. Neuron 75, 58–64. 10.1016/j.neuron.2012.04.038. [PubMed: 22794260]

Willett JA, Cao J, Dorris DM, Johnson AG, Ginnari LA, and Meitzen J (2019). Electrophysiological properties of medium spiny neuron subtypes in the caudate-putamen of prepubertal male and female drd1a-tdTomato line 6 BAC transgenic mice. Eneuro 6. 10.1523/eneuro.0016-19.2019.

Willuhn I, Burgeno LM, Groblewski PA, and Phillips PEM (2014). Excessive cocaine use results from decreased phasic dopamine signaling in the striatum. Nat. Neurosci 17, 704–709. 10.1038/nn.3694. [PubMed: 24705184]

Witten IB, Lin S-C, Brodsky M, Prakash R, Diester I, Anikeeva P, Gradinaru V, Ramakrishnan C, and Deisseroth K (2010). Cholinergic interneurons control local circuit activity and cocaine conditioning. Science 330, 1677–1681. 10.1126/science.1193771. [PubMed: 21164015]

Yan Z, Flores-Hernandez J, and Surmeier DJ (2001). Coordinated expression of muscarinic receptor messenger RNAs in striatal medium spiny neurons. Neuroscience 103, 1017–1024. 10.1016/s0306-4522(01)00039-2. [PubMed: 11301208]

Yorgason JT, Zeppenfeld DM, and Williams JT (2017). Cholinergic interneurons underlie spontaneous dopamine release in nucleus accumbens. J. Neurosci 37, 2086–2096. 10.1523/jneurosci.3064-16.2017. [PubMed: 28115487]

Ztaou S, Maurice N, Camon J, Guiraudie-Capraz G, Kerkerian-Le Goff L, Beurrier C, Liberge M, and Amalric M (2016). Involvement of striatal cholinergic interneurons and M1 and M4 muscarinic receptors in motor symptoms of Parkinson's disease. J. Neurosci 36, 9161–9172. 10.1523/jneurosci.0873-16.2016. [PubMed: 27581457]

Highlights

- NAc acetylcholine signaling correlates with cocaine extinction
- Cocaine extinction decreases glutamatergic presynaptic strength at D1R and D2R MSNs
- Activation of ChINs promotes extinction and associated plasticity
- Inhibition of ChINs blocks extinction and associated plasticity

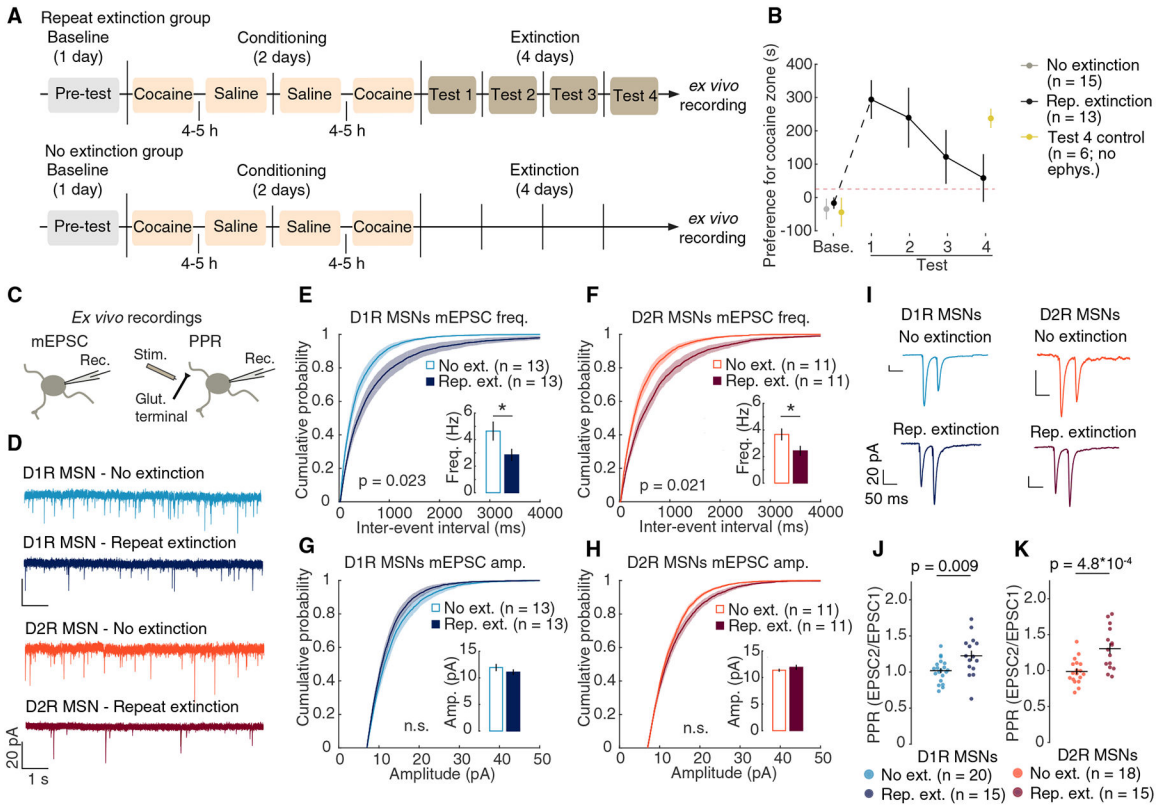

Figure 1. Repeat extinction after cocaine CPP reduces excitatory presynaptic strength at both MSN subtypes in NAc medial shell

(A) Timeline of CPP experiments. Conditioning was followed by either repeat extinction testing (tests 1–4) or no extinction. Brain slices were collected on day 7.

(B) Preference for the cocaine zone, measured as the difference in time spent in the cocaine zone minus time spent in the saline zone. Repeat extinction mice showed preference for the cocaine zone that extinguished across days, $F_{(4,48)} = 7.74$, $p = 6.8*10^{-5}$, for session in one-way repeated measures ANOVA with the five sessions (baseline and tests 1–4) as fixed effect and mouse as random effect). A group of behavior-only control mice that did not undergo extinction testing until the test 4 time point (test 4 control, yellow) maintained preference ($p = 8.9*10^{-4}$ for the baseline vs. test 4 for one-sample t test).

(C) Schematic of *ex vivo* experiments.

(D) Example traces of whole-cell, voltage-clamp mEPSCs.

(E) Cumulative probability of inter-event intervals for mEPSCs at D1R MSNs. Repeat extinction decreased mEPSC frequency in D1R MSNs compared with controls (d = 0.99, p = 0.023 for group in a linear mixed effects regression (LMER) on frequency with group as a fixed effect and cell as random effect. Inset: median frequency of mEPSCs. No extinction, n = 13 cells, 4 mice, 4.7 Hz ± 0.7. Repeat extinction, n = 13 cells, 4 mice, 2.8 Hz ± 0.5).

(F) Cumulative probability of inter-event intervals for mEPSCs at D2R MSNs. Repeat extinction decreased mEPSC frequency in D2R MSNs compared with controls (d = 1.12, p = 0.021 for group in an LMER on frequency. Inset: median frequency of mEPSCs. No extinction, n = 11 cells, 4 mice, 3.7 Hz ± 0.5. Repeat extinction, n = 11 cells, 4 mice, 2.4 Hz ± 0.4).

(G) Cumulative probability of amplitudes for mEPSCs at D1R MSNs. Repeat extinction testing did not affect mEPSC amplitude in D1R MSNs compared with controls (d = −0.43, p = 0.304 for group in an LMER on amplitude. Inset: median amplitude of mEPSCs. No extinction, n = 13 cells, 4 mice, 11.9 pA ± 0.7. Repeat extinction, n = 13 cells, 4 mice, 11.1 pA ± 0.5).

(H) Cumulative probability of amplitudes for mEPSCs at D2R MSNs. Repeat extinction testing did not affect mEPSC amplitude in D2R MSNs compared with controls (d = 0.43, p = 0.345 for group in an LMER on amplitude. Inset: median amplitude of mEPSCs. No extinction, n = 11 cells, 4 mice, 11.4 pA ± 0.3. Repeat extinction, n = 11 cells, 4 mice, 11.9 pA ± 0.5).

(I) Representative electrically evoked EPSCs in D1R and D2R MSNs in response to inter-pulse intervals of 50 ms. Scale bars, 50 ms and 20 pA.

(J) Repeat extinction increased PPR at D1R MSNs compared with controls (d = 0.91, p = 0.009, two-tailed t test. No extinction, n = 20 cells, 3 mice, 1.02 ± 0.04. Repeat extinction, n = 15 cells, 3 mice, 1.23 ± 0.07).

(K) Repeat extinction increased PPR at D2R MSNs compared with controls (d = 1.33, p = $4.8*10^4$, two-tailed t test. No extinction, n = 18 cells, 3 mice, 0.99 ± 0.04. Repeat extinction, n = 15 cells, 3 mice, 1.31 ± 0.08). All error bars are standard error of the mean.

See also Figure S1.

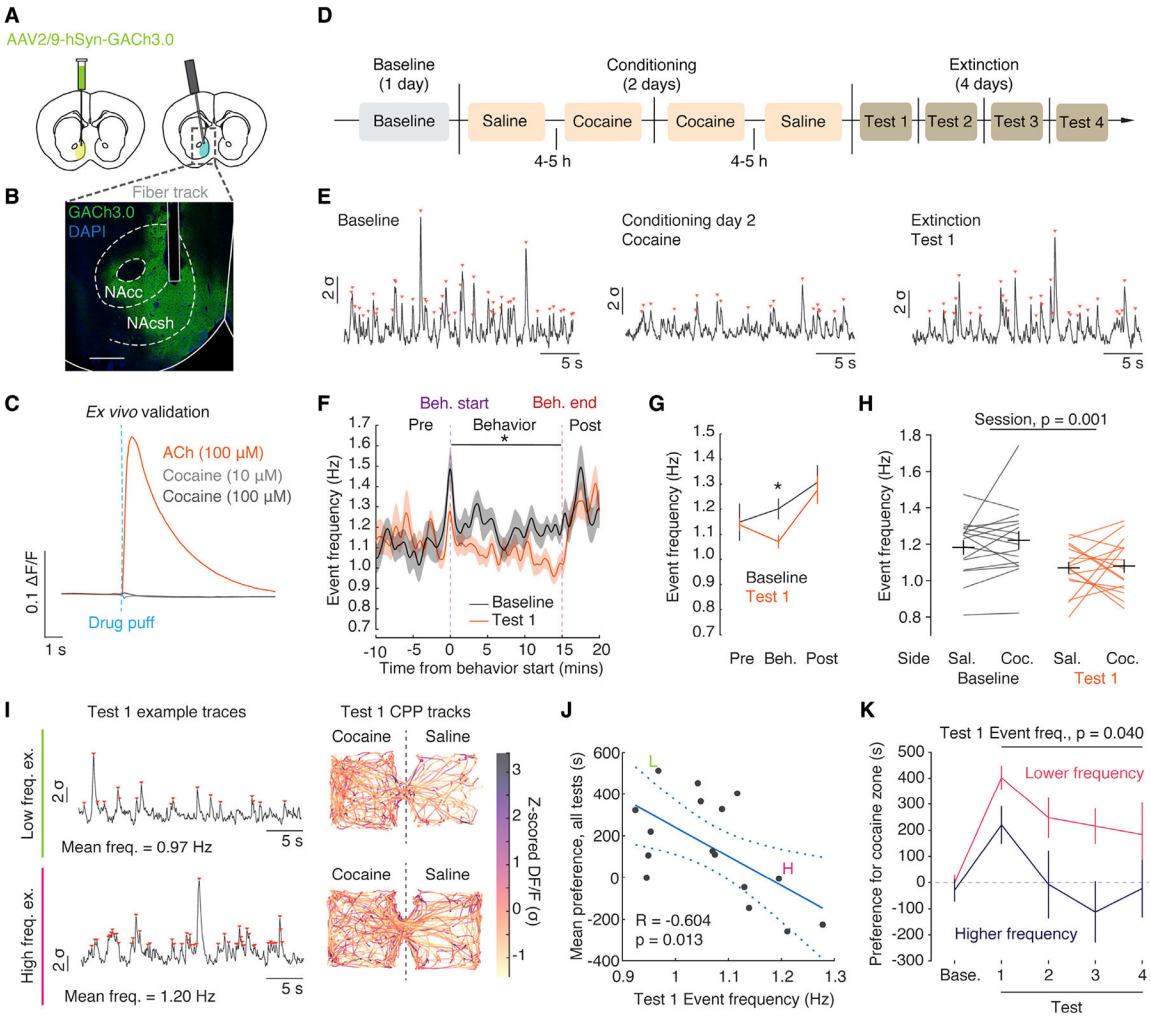

Figure 2. Mice with higher ACh event rate during cocaine extinction exhibit less cocaine preference

(A) AAV2/9-hSyn-GACh3.0 virus was injected into the NAc medial shell. Fibers were implanted above the injection sites for unilateral recordings.

(B) Representative image showing GACh3.0 expression in NAc with fiber placement (NAcc, NAc core; NAcsh, NAc shell). Scale bar, 500 µm.

(C) *Ex vivo* imaging shows tissue expressing GACh3.0 is responsive to ACh puff, but not cocaine.

(D) Timeline of the CPP experiment.

(E) Example z-scored dF/F of GACh3.0 fiber photometry traces from a mouse with demarcated detected events (red triangles) during baseline, cocaine conditioning 2, and test 1.

(F) Mean event frequency calculated with a 30-s moving window before, during, and after baseline (gray) and test 1 (orange) sessions.

(G) Mean event frequencies were significantly decreased during behavior testing (Beh), but not in periods before (Pre) or after (Post) behavior (p = 0.893 for pre-behavior period

pairwise t test of baseline and test 1; p = 0.013 for behavior period; p = 0.730 for post-behavior period).

(H) Mean event frequency is not different between cocaine- and saline-conditioned zones on baseline or test 1 ($F_{(1,45)}$ = 12.68, p = 0.001 for session; $F_{(1,45)}$ = 0.47, p = 0.498 for chamber side; $F_{(1,45)}$ = 0.17, p = 0.684 for session*chamber side in repeated measures ANOVA on mean event frequency with session (test 1 vs. baseline), chamber side (saline vs. cocaine), and their interaction as fixed effects and mouse as random effect).

(I) Left: z-scored dF/F of GACh3.0 recorded during test 1 from example mice with either low event frequency (top) or high event frequency (bottom). Right: Example CPP test tracks from the same mice during test 1, colored with Z score value of GACh3.0 fluorescence. Scale bar is constrained to 1st and 99th percentile values of Z score values from the two mice.

(J) Across individuals, event frequency on test 1 is significantly negatively correlated with mean preference for the cocaine zone on tests 1–4 (R = −0.604; p = 0.013).

(K) Mean preference for the cocaine zone when mice are median split by test 1 frequency (lower frequency, pink, n = 8; higher frequency, purple, n = 8). Event frequency on test 1 is significantly predictive of preference on tests 1–4 ($F_{(1,14)}$ = 5.10, p = 0.040 for the median split group in repeated measures ANOVA on preference with group, test number, and their interaction as fixed effects and mouse as random effect). All error bars are standard error of the mean.

See also Figures S2–S4.

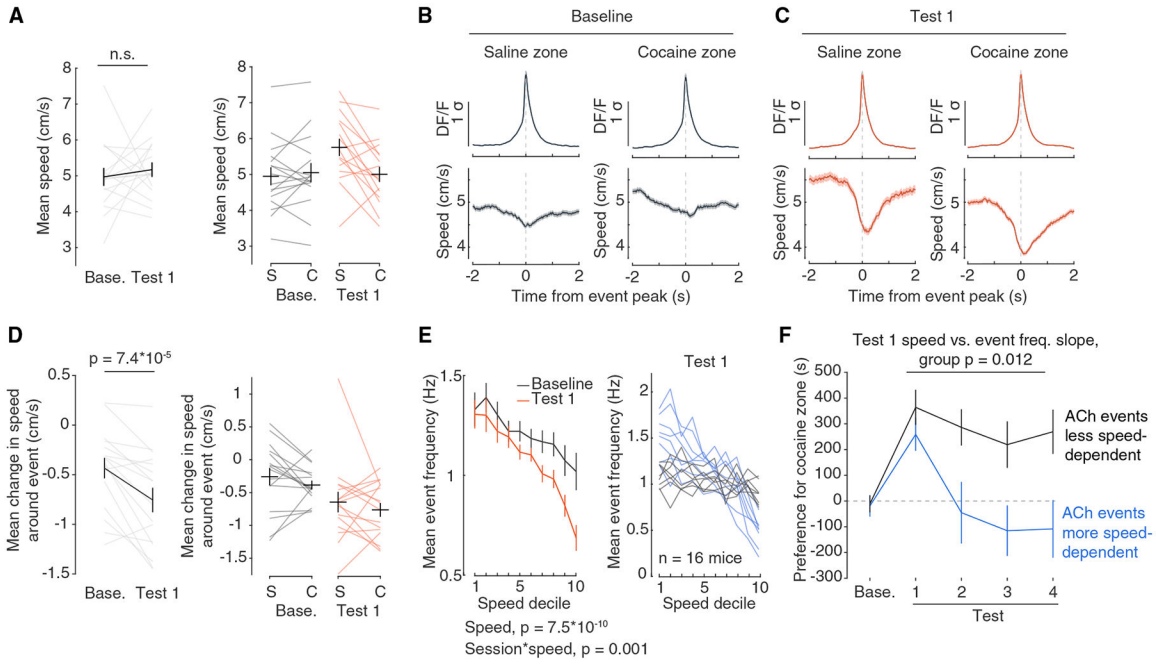

Figure 3. Mice with a stronger relationship between ACh events and speed after conditioning exhibit less cocaine preference

(A) Mean speed during baseline and test 1 sessions (left) and broken down by chamber side (right). Mice maintain similar speeds between baseline and test 1 and regardless of chamber side ($F_{(1,45)}$ = 2.88, p = 0.097 for session; $F_{(1,45)}$ = 2.19, p = 0.146 for chamber side; $F_{(1,45)}$ = 3.74, p = 0.059 for session*chamber side in repeated measures ANOVA on mean speed with session (test 1 vs. baseline), chamber side (saline vs. cocaine), and their interaction as fixed effects and mouse as random effect).

(B) Top: Mean z-scored dF/F trace of GACh3.0 signal centered at peak time for all significant events across all mice in the saline zone (left) and cocaine zone (right) during baseline. Bottom: Mean speed across all events from all mice over the same time period in the saline zone (left) or cocaine zone (right) during baseline (n = 8,589 events in saline zone, 8,610 events in cocaine zone).

(C) Same as (B), but for test 1 (n = 5,057 events in saline zone, 10,286 events in cocaine zone).

(D) Mean change in speed around ACh events during baseline and test 1 (left) and broken down by chamber side (right). Events coincide with larger decreases in speed on test 1 than baseline ($F_{(1,45)}$ = 19.04, p = $7.4*10^{-5}$ for session in repeated measures ANOVA on change in speed with session, chamber side, and their interaction as fixed effects and mouse as random effect). Changes in speed around time of events were calculated as mean speed in a 1.5-s window beginning 0.5 s before event peak and ending 1 s after event peak, baseline subtracted with the mean speed in a 1-s window starting 2 s before the event peak.

(E) Left: Mean event frequency by speed decile during baseline and test 1. Speed deciles are calculated for each mouse across all speed data from baseline and test 1. Event frequency is negatively modulated by speed, and to a greater extent at test 1 than at baseline (d = −0.75, p = $7.5*10^{-10}$ for speed; d = 0.41, p = 0.001 for session*speed in an LMER with session, speed decile, and their interaction as fixed effects and mouse as random effect). Right: Mean

event frequency by speed decile on test 1 for individual mice. Individual traces are colored by median split of slope to highlight differences in speed dependency (black: less negative speed vs. frequency slope; blue: more negative slope).

(F) Mean preference for the cocaine zone when mice are median split by the slopes of the speed decile vs. test 1 mean event frequency (less speed dependence, black, n = 8; more speed dependence, blue, n = 8). Speed decile slope is significantly predictive of preference on tests 1–4 ($F_{(1,14)} = 8.34$, $p = 0.012$, for the median split group in repeated measures ANOVA with group, test number, and their interaction as fixed effects and mouse as random effect). All error bars are standard error of the mean.

See also Figure S5.

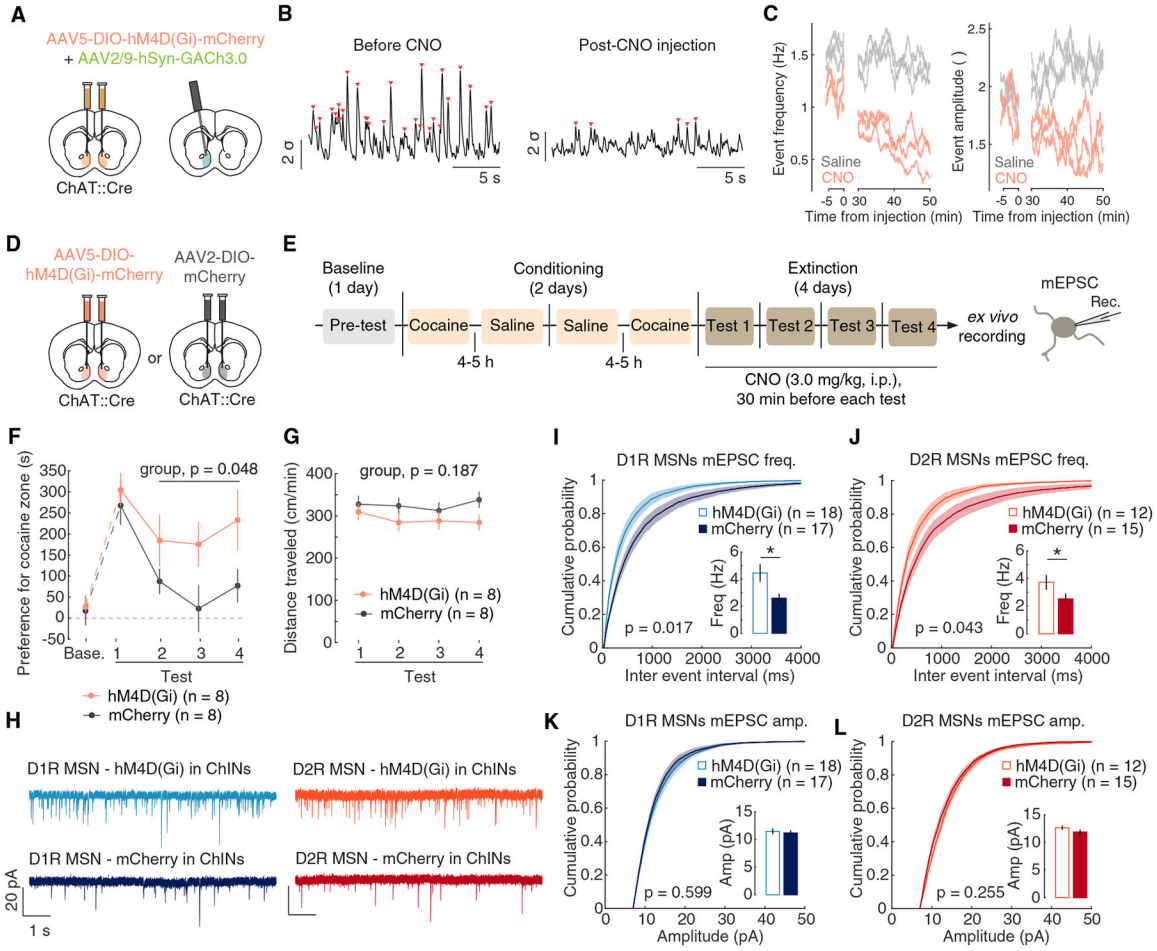

Figure 4. ChIN inhibition during cocaine extinction preserves preference and blocks extinction-associated plasticity

(A) Both Cre-dependent AAV5-hM4D(G_i)-mCherry and AAV2/9-hSyn-GACh3.0 virus were injected into the NAc medial shell.

(B) Example z-scored dF/F of GACh3.0 fiber photometry traces from a mouse with demarcated detected events (red triangles) before and 40 min after CNO injection (3.0 mg/kg, i.p.).

(C) Mean ACh event frequency (left) and event amplitude (right) before and after injection of either CNO (orange) or saline (gray). Each line is a 120-s moving average of a recording from the same mouse.

(D) Either Cre-dependent AAV5-hM4D(G_i)-mCherry or Cre-dependent AAV2-mCherry virus was injected bilaterally into the NAc of ChAT::Cre×drd1a-tdTomato or ChAT::Cre×drd2-GFP mice.

(E) Timeline of CPP experiment. Both groups underwent repeat extinction tests and received an i.p. injection of CNO (3.0 mg/kg) 30 min before each test. Brain slices were collected immediately after test 4.

(F) Inhibition of ChINs increased preference for the cocaine-paired chamber compared with controls over tests 2–4 ($F_{(1,14)} = 4.96$, $p = 0.043$ for group in multi-factor, repeated measures ANOVA on preference on tests 2–4 with group (hM4D(G_i) vs. mCherry control), session

(tests 2–4), and their interaction as fixed effects and mouse as random effect). Separate one-way ANOVAs in either group showed session-dependent decay in preference in controls only ($F_{(1,7)}$ = 8.77, p = 0.007, for session in one-way repeated measures ANOVA on preference in controls only with session (tests 1–4) as fixed effect and mouse as random effect; $F_{(1,7)}$ = 1.39, p = 0.25, for session in one-way repeated measures ANOVA on preference in DREADD mice only).

(G) Inhibition of ChINs did not affect locomotion during extinction tests ($F_{(1,14)}$ = 1.928, p = 0.187 for group in multi-factor, repeated measures ANOVA on distance traveled with group, session, and their interaction as fixed effects and mouse as random effect).

(H) Example traces of whole-cell, voltage-clamp mEPSCs.

(I) Cumulative probability of inter-event intervals for mEPSCs at D1R MSNs. ChIN inhibition mice showed higher mEPSC frequency at D1R MSNs compared with controls (d = 0.83, p = 0.017 for group in an LMER on frequency with group as a fixed effect and cell as random effect. Inset: median frequency of mEPSCs. hM4D(G_i), n = 18 cells, 3 mice, 4.5 ± 0.7 Hz. mCherry, n = 17 cells, 3 mice, 2.6 ± 0.3 Hz).

(J) Cumulative probability of inter-event intervals for mEPSCs at D2R MSNs. ChIN inhibition mice showed higher mEPSC frequency at D2R MSNs compared with controls (d = 0.80, p = 0.043 for group in an LMER on frequency. Inset: median frequency of mEPSCs. hM4D(G_i), n = 12 cells, 3 mice, 3.7 ± 0.5 Hz. mCherry, n = 15 cells, 4 mice, 2.5 ± 0.4 Hz).

(K) Cumulative probability of amplitudes for mEPSCs at D1R MSNs. ChIN inhibition did not affect mEPSC amplitudes at D1R MSNs compared with controls (d = 0.18, p = 0.599 for group in an LMER on amplitude. Inset: median amplitude of mEPSCs. hM4D(G_i), n = 18 cells, 3 mice, 11.5 ± 0.5 pA. mCherry, n = 17 cells, 3 mice, 11.2 ± 0.5 pA).

(L) Cumulative probability of amplitudes for mEPSCs at D2R MSNs. ChIN inhibition did not affect mEPSC amplitudes at D2R MSNs compared with controls (d = 0.45, p = 0.255 for group in an LMER on frequency. Inset: median amplitude of mEPSCs. hM4D(G_i), n = 12 cells, 3 mice, 12.6 ± 0.4 pA. mCherry, n = 15 cells, 4 mice, 11.9 ± 0.4 pA). All error bars are standard error of the mean.

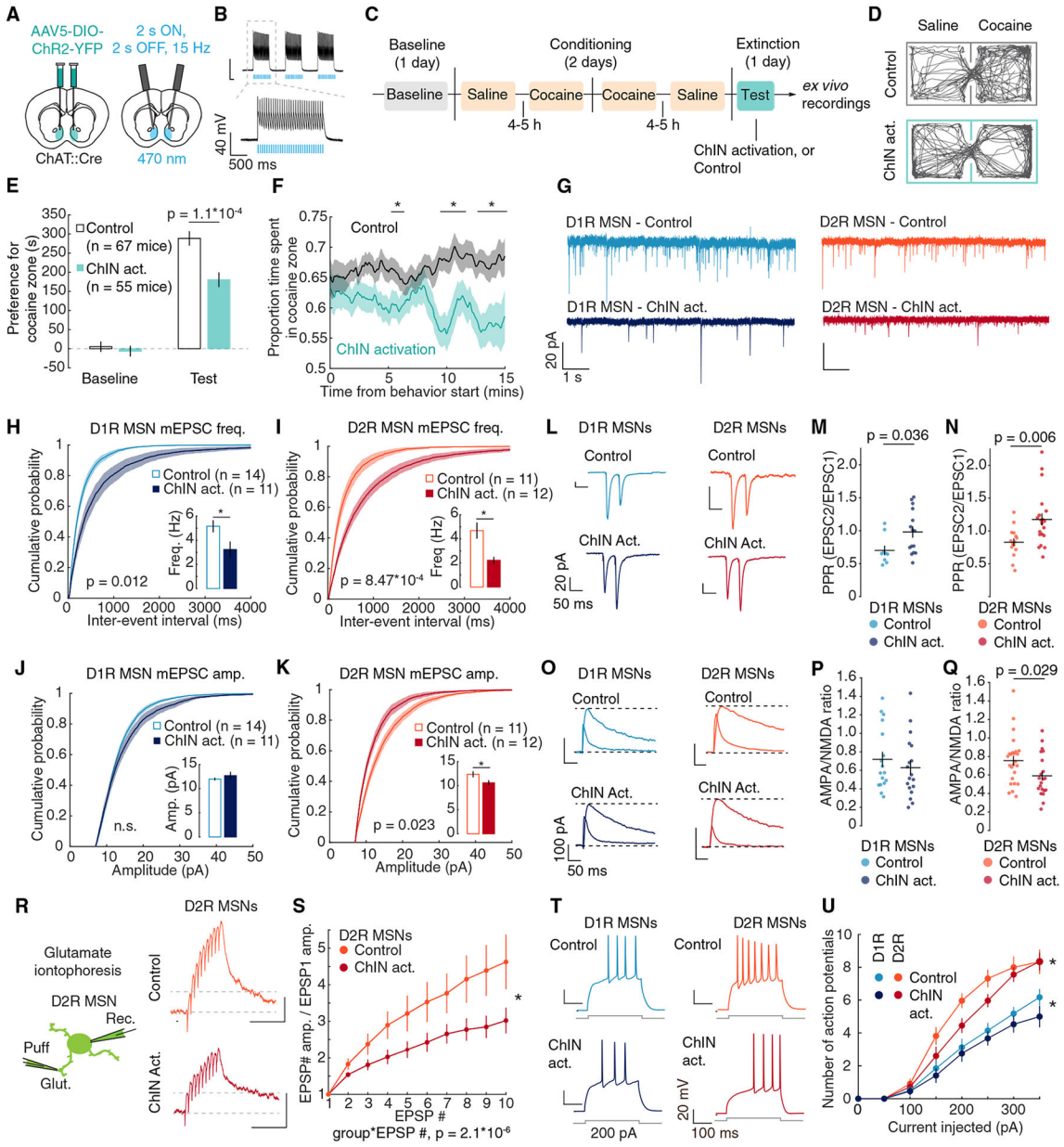

Figure 5. ChIN activation during cocaine extinction weakens presynaptic glutamatergic synapses in both MSN subtypes, with D2R MSN-specific postsynaptic effects

(A) Cre-dependent AAV5-ChR2-YFP virus was injected bilaterally into the NAc of ChAT::Cre×drd1a-tdTomato or ChAT::Cre×drd2-GFP mice. Fibers were implanted above the injection sites.

(B) Whole-cell current clamp recordings confirm functionality of ChR2 in NAc ChINs.

(C) Timeline of CPP experiment. ChIN activation group received optogenetic stimulation during extinction testing (447 nm, 15 Hz, 5-ms pulse duration, 2-s light on interleaved with a 2-s light off). Immediately after the test, brain slices were collected.

(D) Example locomotor tracks during extinction testing.

(E) ChIN activation decreased preference for the cocaine-paired chamber compared with control mice ($F_{(1,118)}$ = 10.88, p = 0.001 for session*group interaction; multi-factor, repeated

measures ANOVA with genotype, group (ChIN activation vs. control), session (baseline vs. test), and their interactions as fixed effects, and mouse as random effect; $p = 0.550$ for post hoc test of group on baseline, $p = 1.1*10^{-4}$ for group on test, Holm-Sidak's post hoc test).
(F) Mean proportions of time spent in the cocaine zone in the test session, plotted as moving means with a centered 2-min window. ChIN activation reduced preference as a function of time ($p = 0.025$ for group*time interaction in an LMER with group (ChIN activation vs. control), time (1 min non-overlapping, unsmoothed bins), and their interaction as fixed effects and mouse as random effect; $p < 0.05$ at mins 6, 10–11, 13–15 in post hoc pairwise t-tests of each min between groups with Holm's correction).
(G) Example traces of whole-cell, voltage-clamp mEPSCs.
(H) Cumulative probability of inter-event intervals for mEPSCs at D1R MSNs. ChIN activation decreased mEPSC frequency at D1R MSNs compared with controls ($d = 1.14$, $p = 0.012$ for group in an LMER on frequency with group (ChIN activation vs. control) as a fixed effect and cell as random effect. Inset: median frequency of mEPSCs. Control, n = 14 cells, 13 mice, 5.2 ± 0.5 Hz. ChIN activation, n = 11 cells, 10 mice, 3.2 ± 0.7 Hz).
(I) Cumulative probability of inter-event intervals for mEPSCs at D2R MSNs. ChIN activation decreased mEPSC frequency at D2R MSNs compared with controls ($d = 1.70$, $p = 8.5*10^{-4}$ for group in an LMER on frequency. Inset: median frequency of mEPSCs. Control, n = 11 cells, 6 mice, 4.7 ± 0.7 Hz. ChIN activation, n = 11 cells, 6 mice, 2.2 ± 0.3 Hz).
(J) Cumulative probability of amplitudes for mEPSCs at D1R MSNs. ChIN activation did not affect mEPSC amplitude in D1R MSNs compared with controls ($d = 0.34$, $p = 0.429$ for group in an LMER on amplitude. Inset: median amplitude of mEPSCs. Control, n = 14 cells, 13 mice, 12.0 ± 0.3 pA. ChIN activation, n = 11 cells, 10 mice, 12.7 ± 0.8 pA).
(K) Cumulative probability of amplitudes for mEPSCs at D2R MSNs. ChIN activation decreased mEPSC amplitudes in D2R MSNs compared with controls ($d = -1.07$, $p = 0.023$ for group in an LMER on amplitude. Inset: median amplitude of mEPSCs. Control, n = 11 cells, 9 mice, 12.4 ± 0.6 pA. ChIN activation, n = 11 cells, 6 mice, 10.6 ± 0.6 pA).
(L) Representative electrically evoked EPSCs in response to interpulse intervals of 50 ms.
(M) ChIN activation increased PPR at D1R MSNs compared with controls ($d = 0.99$, $p = 0.036$, two-tailed t test. Control, n = 9 cells, 5 mice, 0.70 ± 0.07. ChIN activation, n = 15 cells, 5 mice, 0.98 ± 0.09).
(N) ChIN activation increased PPR at D2R MSNs compared with controls ($d = 1.04$, $p = 0.006$, two-tailed t test. Control group, n = 15 cells, 8 mice, 0.83 ± 0.06. ChIN activation group, n = 20 cells, 8 mice, 1.18 ± 0.09).
(O) Representative traces of electrically evoked AMPA and NMDA receptor-mediated currents measured in voltage clamp at +40 mV.
(P) ChIN activation did not affect AMPA/NMDA ratio at D1R MSNs compared with controls ($d = 0.270$, $p = 0.431$, two-tailed t test. Control, n = 17 cells, 9 mice, 0.72 ± 0.08. ChIN activation, n = 18 cells, 7 mice, 0.63 ± 0.08).
(Q) ChIN activation reduced AMPA/NMDA ratio at D2R MSNs compared with controls ($d = 0.67$, $p = 0.029$, two-tailed t test. Control, n = 25 cells, 13 mice, 0.76 ± 0.05. ChIN activation, n = 21 cells, 10 mice, 0.59 ± 0.05).
(R) Schematic of iontophoretic application of glutamate to D2R MSN dendrites and example traces of postsynaptic response.

(S) Group mean magnitudes of EPSP response to each application of glutamate, normalized to the first EPSP. Cells from mice that had received ChIN activation during extinction show significantly less summation of EPSPs ($d = 0.80$, $p = 2.1*10^{-6}$ for group*EPSP number in an LMER with group (ChIN activation vs. control), EPSP number, and their interaction as fixed effects and cell as random effect. Control n = 10 cells, 3 mice. ChIN activation n = 7 cells, 3 mice).

(T) Representative traces of evoked action potentials during a 300 ms, 200 pA current injection.

(U) Plots of mean number of evoked action potentials vs. injected current in D1R MSNs (blues) and D2R MSNs (reds). For both MSN subtypes, there was a significant interaction effect between group and current ($d = 0.28$, $p = 0.046$ for current*group interaction for D1R MSNs in an LMER with group (ChIN activation vs. control), injected current, and their interaction as fixed effects and cell as random effect; $p = 0.044$ in D1R MSNs for pairwise group comparison on slope of current-spike response. Control n = 17 cells, 5 mice. ChIN activation n = 18 cells, 4 mice; $d = 0.32$, $p = 0.040$ for current*group interaction for D2R MSNs in an LMER; $p = 0.038$ in D2R MSNs for pairwise group comparison on slope of current-spike response. Control n = 16 cells, 7 mice. ChIN activation n = 15 cells, 4 mice). All error bars are standard error of the mean.

See also Figures S6 andS7.

KEY RESOURCES TABLE

REAGENT or RESOURCE	SOURCE	IDENTIFIER
Antibodies		
Choline acetyltransferase	Millipore	Cat#: AB144P; RRID: AB_2079751
Donkey anti-sheep IgG (H + L) cross-adsorbed secondary antibody, Alexa Fluor™ 568	Invitrogen	Cat#A-11004; RRID:AB_2534104
GFP antibody	Millipore	Cat#: NB600-308; RRID:AB_10003058
Fluoromount-G	Southern Biotech	Cat#: 0100-01
GFP Recombinant Rabbit Monoclonal Antibody	Invitrogen	Cat#: G10362; RRID: AB_2536526
Alexa Fluor® 488 AffiniPure Donkey Anti-Rabbit IgG (H + L)	Jackson Immuno	Cat#: 711-545-152; RRID: AB_2313584
Bacterial and virus strains		
AAV5-EF1a-DIO-hChR2(H134R)-EYFP-WPRE-HGHpA	Viral prep, Princeton Neuroscience Viral Core. Plasmid, Addgene.	Addgene plasmid# 20298; RRID: Addgene_20298
AAV5-hSyn-DIO-hM4D(Gi)-mCherry	Viral prep, Princeton Neuroscience Viral Core. Plasmid, Addgene.	Addgene plasmid# 44362; RRID: Addgene_44362
AAV2-EF1a-DIO-mCherry-WPRE-HGHpA	Viral prep, Princeton Neuroscience Viral Core. Plasmid, Addgene.	Addgene plasmid# 20299; RRID: Addgene_20299
AAV2/9-hSyn-GRAB_ACh3.0-WPRE-hGHpA	Viral prep, Princeton Neuroscience Viral Core. Plasmid, Addgene.	Addgene plasmid# 121922; RRID: Addgene_121922
Chemicals, peptides, and recombinant proteins		
Cocaine hydrochloride	Sigma-Aldrich	Cat#: C5776; CAS#: 53-21-4
Clozapine *N*-oxide (CNO) dihydrochloride	HelloBio	Cat#: HB6149; CAS#: 2250025-93-3
Tetrodotoxin citrate	Tocris	Cat#: 1069; CAS#: 18660-81-6
D-AP5	Tocris	Cat#: 0106; CAS#: 79055-68-8
Picrotoxin	Sigma-Aldrich	Cat#: P1675; CAS#: 124-87-8
Alexa Fluor™ 594 Hydrazide	Invitrogen	Cat#: A10438
Acetylcholine chloride	Sigma-Aldrich	Cat#: A6625; CAS#: 60-31-1
Critical commercial assays		
RNAscope Multiplex Fluorescent Assay	Advanced Cell Diagnostics	Cat#: 323110
Mm-Drd1a-C1	Advanced Cell Diagnostics	Cat#: 406491-C1
Mm-Drd2-C2	Advanced Cell Diagnostics	Cat#: 406501-C2
Mm-tdTomato-C3	Advanced Cell Diagnostics	Cat#: 317041-C3
TSA Plus Fluorescence Palette Kit	Perkin Elmer	Cat#: NEL760001KT
Deposited data		
Data	this paper	10.6084/m9.figshare.19596826
Experimental models: Organisms/strains		
Mouse: B6.129S6-Chattm2(cre)Lowl/J	The Jackson Laboratory	Stock#: 006410; RRID: IMSR_JAX:006410
Mouse: B6.Cg-Tg(Drd1a-tdTomato)6Calak/J	The Jackson Laboratory	Stock#: 016204; RRID: IMSR_JAX:016204
Mouse: Tg(Drd2-EGFP)S118Gsat/Mmnc	Mutant Mouse Research & Resource Centers	Stock#: 000230-UNC; RRID: MMRRC_000230-UNC
Software and algorithms		
MATLAB	Mathworks	https://www.mathworks.com/products/matlab.html

REAGENT or RESOURCE	SOURCE	IDENTIFIER
pClamp	Molecular Devices	https://www.moleculardevices.com/products
Stimfit	Guzman et al. (2014)	https://github.com/neurodroid/stimfit
EthoVision	Noldus	https://www.noldus.com/ethovision-xt
Custom analysis code	This paper	Database: 10.6084/m9.figshare.19596826